Measurement of the forward Z boson production cross-section in pp collisions at $\sqrt{s} = 7\,\text{TeV}$

The LHCb collaboration

E-mail: ronan.wallace@cern.ch

ABSTRACT: A measurement of the production cross-section for Z bosons that decay to muons is presented. The data were recorded by the LHCb detector during pp collisions at a centre-of-mass energy of 7 TeV, and correspond to an integrated luminosity of $1.0\,\text{fb}^{-1}$. The cross-section is measured for muons in the pseudorapidity range $2.0 < \eta < 4.5$ with transverse momenta $p_\text{T} > 20\,\text{GeV}/c$. The dimuon mass is restricted to $60 < M_{\mu^+\mu^-} < 120\,\text{GeV}/c^2$. The measured cross-section is

$$\sigma_{Z\to\mu^+\mu^-} = (76.0 \pm 0.3 \pm 0.5 \pm 1.0 \pm 1.3)\,\text{pb}$$

where the uncertainties are due to the sample size, systematic effects, the beam energy and the luminosity. This result is in good agreement with theoretical predictions at next-to-next-to-leading order in perturbative quantum chromodynamics. The cross-section is also measured differentially as a function of kinematic variables of the Z boson. Ratios of the production cross-sections of electroweak bosons are presented using updated LHCb measurements of W boson production. A precise test of the Standard Model is provided by the measurement of the ratio

$$\frac{\sigma_{W^+\to\mu^+\nu_\mu} + \sigma_{W^-\to\mu^-\bar{\nu}_\mu}}{\sigma_{Z\to\mu^+\mu^-}} = 20.63 \pm 0.09 \pm 0.12 \pm 0.05,$$

where the uncertainty due to luminosity cancels.

KEYWORDS: Electroweak interaction, Hadron-Hadron Scattering, proton-proton scattering, QCD, Forward physics

JHEP08(2015)039

Contents

1 Introduction

Measurements of the total and differential cross-sections for the production of Z bosons in pp collisions test the Standard Model (SM) and provide constraints on parton density functions (PDFs) of the proton.[1] Theoretical predictions for these cross-sections are available at next-to-next-to-leading order (NNLO) in perturbative quantum chromodynamics (pQCD) [1–5]. The dominant uncertainty on these predictions reflects the uncertainties on the PDFs, which vary as functions of the kinematic variables studied. The forward acceptance of the LHCb detector allows the PDFs to be constrained at Bjorken-x values down to 10^{-4} [6]. Ratios of the W and Z cross-sections provide precise tests of the SM as the sensitivity to the PDFs in the theoretical calculations is reduced and many of the experimental uncertainties cancel.

---

[1]Throughout this article Z represents both resonant production of Z bosons and off-mass-shell photons.

LHCb has measured the Z boson production cross-section at $\sqrt{s} = 7\,\text{TeV}$ using decays to muon pairs in a data set corresponding to $37\,\text{pb}^{-1}$ [7], and using electron [8] and tau lepton [9] pairs in a data set of $1.0\,\text{fb}^{-1}$. Production cross-sections of W bosons and the W^+/W^- cross-section ratio have been measured in the muon channel [10] with the $1.0\,\text{fb}^{-1}$ data set. Similar measurements have also been performed by the ATLAS [11] and CMS [12] collaborations.

The analysis described here is an update of the one described in ref. [7], using a total integrated luminosity of about $1.0\,\text{fb}^{-1}$. This increases statistical precision and allows better control of systematic uncertainties, with the result that the total uncertainties on the measurements are significantly reduced. Measurements are performed for muons with transverse momentum $p_{\text{T}} > 20\,\text{GeV}/c$ and pseudorapidity in the range $2.0 < \eta < 4.5$. In the case of Z boson measurements, the invariant mass of the two muons is required to be in the range $60 < M_{\mu^+\mu^-} < 120\,\text{GeV}/c^2$. These kinematic requirements define the fiducial region of the measurement and in this article are referred to as the fiducial requirements. Total cross-sections are presented as well as differential cross-sections as functions of the Z boson rapidity y_Z, $p_{T,Z}$ and ϕ_Z^*. Here ϕ_Z^* is defined as [13]

$$\phi_Z^* \equiv \frac{\tan\left(\phi_{\text{acop}}/2\right)}{\cosh\left(\Delta\eta/2\right)}. \tag{1.1}$$

The angle $\phi_{\text{acop}} = \pi - |\Delta\phi|$ depends on the difference $\Delta\phi$ in azimuthal angle between the two muon momenta, while the difference between their pseudorapidities is denoted by $\Delta\eta$.

The W boson cross-sections given in ref. [10] are re-evaluated using a more precise determination of the event trigger efficiency. The cross-sections are presented as a function of the η of the muon from the W boson decay. The values presented here supersede those of ref. [10].

This paper is organised as follows: section 2 describes the LHCb detector; sections 3 and 4 detail the selection of Z boson candidates, the Z boson cross-section definition and relevant sources of systematic uncertainty; section 5 presents the results and section 6 concludes the paper. Appendices A and B provide tables of differential cross-sections and correlations between these measurements.

2 Detector and data set

The LHCb detector [14, 15] is a single-arm forward spectrometer covering the pseudorapidity range $2 < \eta < 5$, designed for the study of particles containing b or c quarks. The detector includes a high-precision tracking system consisting of a silicon-strip vertex detector surrounding the pp interaction region [16], a large-area silicon-strip detector located upstream of a dipole magnet with a bending power of about $4\,\text{Tm}$, and three stations of silicon-strip detectors and straw drift tubes [17] placed downstream of the magnet. The tracking system provides a measurement of momentum, p, of charged particles with a relative uncertainty that varies from 0.5% at low momentum to 1.0% at $200\,\text{GeV}/c$. The minimum distance of a track to a primary vertex, the impact parameter, is measured with a resolution of $(15 + 29/p_{\text{T}})\,\mu\text{m}$, where p_{T} is the component of the momentum transverse

to the beam, in GeV/c. Different types of charged hadrons are distinguished using information from two ring-imaging Cherenkov detectors [18]. Photons, electrons and hadrons are identified by a calorimeter system consisting of a scintillating-pad detector (SPD), preshower detectors, an electromagnetic calorimeter and a hadronic calorimeter. Muons are identified by a system composed of alternating layers of iron and multiwire proportional chambers [19]. The online event selection is performed by a trigger [20], which consists of a hardware stage, based on information from the calorimeter and muon systems, followed by a software stage, which applies a full event reconstruction. A requirement that prevents events with high occupancy from dominating the processing time of the software trigger is also applied. This is referred to as the global event cut (GEC) in this article.

The measurement presented here is based on pp collision data collected at a centre-of-mass energy of 7 TeV. The integrated luminosity amounts to 975 ± 17 pb^{-1}. The absolute luminosity scale was measured during dedicated data taking periods, using both Van der Meer scans [21] and beam-gas imaging methods [22]. Both methods give similar results, which are combined to give the final luminosity estimate with an uncertainty of 1.7% [23]. This analysis uses the same data set as in ref. [10].

Several samples of simulated data are produced to estimate contributions from background processes, to cross-check efficiencies and to unfold data for detector-related effects. The Pythia generator [24, 25], configured as in ref. [26] with the CTEQ6L1 [27, 28] parameterisation for the PDFs, is used to simulate $b\bar{b}$, $c\bar{c}$, WW, $t\bar{t}$ and Z production. All generated events are passed through a detector simulation based on Geant4 [29], followed by LHCb-specific trigger emulation and event reconstruction.

The results of the analysis are compared to theoretical predictions calculated with the Fewz [30, 31] generator at NNLO for the PDF sets ABM12 [32], CT10 [33], HERA1.5 [34], JR09 [35], MSTW08 [36], and NNPDF3.0 [37]. Comparisons are also made to the ResBos [38–40] and Powheg [41] generators configured with the CT10 PDF set. ResBos includes an approximate NNLO calculation, plus a next-to-next-to-leading logarithm approximation for the resummation of the soft gluon radiation. Powheg provides a next-to-leading order (NLO) calculation interfaced to a parton shower, in this case performed by Herwig [42, 43]. The results are also compared to the predictions from MC@NLO [44, 45], which is interfaced with different generators to simulate the parton shower. Parton showering is performed using Herwig [42, 43], with different values for the root mean-square-deviation of the intrinsic k_T, and Herwiri [46–48], which is based on infrared-improved [49] DGLAP-CS [50–55] theory. All calculations are performed with the renormalisation and factorisation scales set to the electroweak boson mass. Scale uncertainties are estimated by varying these scales by factors of two around the boson mass [56]. Total uncertainties correspond to the PDF and α_s uncertainties at 68.3% confidence level and scale uncertainties, added in quadrature.

3 Event selection

Events considered in this analysis are selected by the muon trigger. At the hardware stage, this trigger requires a muon with $p_T > 1.5$ GeV/c and imposes an upper limit of 600 hits in the SPD sub-detector. At the software stage, a muon with $p_T > 10$ GeV/c is required.
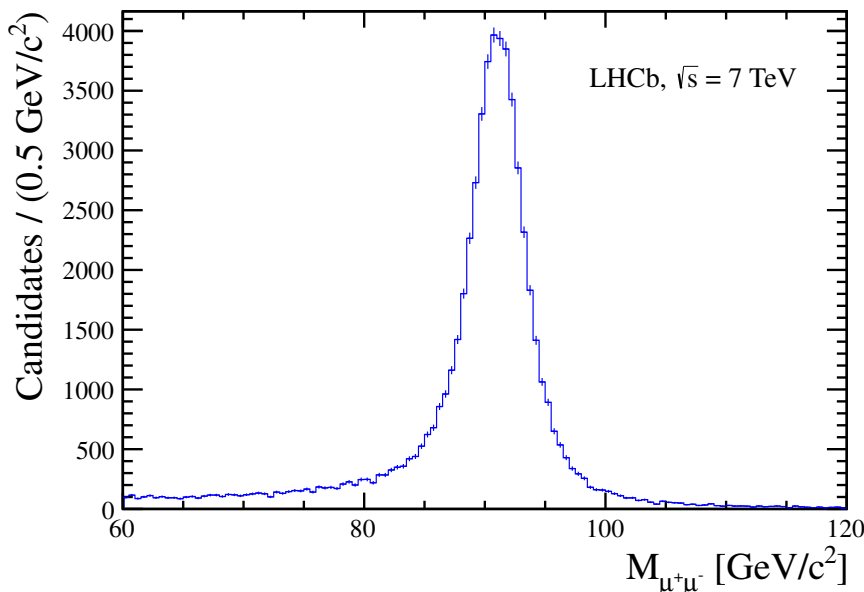
Figure 1. Invariant mass of dimuon candidates.

The muon track must also satisfy additional track quality criteria. Candidate events are selected by requiring a pair of well-reconstructed particles of opposite charge, identified as muons, that also pass the fiducial requirements [7]. In total, $58\,466$ Z boson candidates are selected and their invariant mass distribution is shown in figure 1.

The background contamination in the candidate sample is low. Five background sources are investigated: decays of heavy flavour hadrons, hadron misidentification, $Z \to \tau^+\tau^-$ decays, $t\bar{t}$ and W^+W^- production. Unlike muons from signal, muons arising from decays of heavy flavour hadrons are neither directly produced at the primary interaction vertex, nor are they isolated particles. Using the techniques from ref. [7], the contribution from this background is estimated from the data to be 227 ± 32 events, which amounts to 0.4% of the candidate sample. The contribution from hadrons that decay in flight or have sufficient energy to traverse the calorimeters and be detected in the muon stations is studied in randomly triggered data, as described in ref. [7], and determined to be 116 ± 45 events, which is 0.2% of the candidate sample. Other electroweak and QCD backgrounds are estimated using PYTHIA simulation [25] and normalised to the measured total cross-sections for $Z \to \tau^+\tau^-$ decays [57, 58], $t\bar{t}$ [59, 60] and W^+W^- [61, 62] production. The estimate for these sources is 66 ± 6 events, or 0.1% of the candidate sample. In total, the background is estimated to be 409 ± 56 events, or 0.7% of the candidate sample.

The purity, defined to be the ratio of signal to total candidate events, is $\rho = 0.993 \pm 0.002$. It is assumed to be constant as a function of y_Z, $p_{T,Z}$ and ϕ_Z^*. A systematic uncertainty, discussed later, is assigned to allow for possible inaccuracies in this assumption.

4   Cross-section measurement

Cross-sections are quoted in the kinematic range defined by the measurement and are corrected for quantum electrodynamic (QED) final-state radiation (FSR) in order to provide a

consistent comparison with NLO and NNLO QCD predictions. No corrections are applied for initial-state radiation, electroweak effects, nor their interplay with QED effects. The cross-section in a given bin i of y_Z, $p_{T,Z}$ or ϕ_Z^*, with both final-state muons inside the fiducial region, is measured as

$$\sigma_{Z\to\mu^+\mu^-}(i) = \frac{\rho}{\mathcal{L}} \frac{f_{\text{FSR}}(i)}{\varepsilon_{\text{GEC}}(i)} \sum_j U_{ij} \left(\sum_k \frac{1}{\varepsilon(\eta_k^{\mu^+}, \eta_k^{\mu^-})} \right)_j . \tag{4.1}$$

The indices i and j run over the bins of the variable under study. The index k runs over the candidates contributing to bin j. The total muon reconstruction efficiency for an event is given by $\varepsilon(\eta_k^{\mu^+}, \eta_k^{\mu^-})$, which is dependent on the pseudorapidity of the two muons. The matrix U corrects the data for bin migrations due to detector resolution effects. It is determined using an unfolding procedure, which is described in section 4.4. The efficiency of the requirement on the number of SPD hits in the hardware trigger is denoted by ε_{GEC}. The correction factors for QED final-state radiation are denoted by $f_{\text{FSR}}(i)$ and are determined for each bin. The integrated luminosity is denoted by $\mathcal{L}$. Though not entering the expression for the cross-section, an uncertainty due to the beam energy is assigned to all cross-sections. More detail on these individual components is given below. Once the binned cross-sections are determined, they are summed to give the total cross-section

$$\sigma_{Z\to\mu^+\mu^-} = \sum_i \sigma_{Z\to\mu^+\mu^-}(i). \tag{4.2}$$

The most precise estimate of the total cross-section is obtained by summing the cross-sections as a function of rapidity, where uncertainties due to data unfolding are negligible.

4.1 Muon reconstruction efficiencies

The data are corrected for efficiency losses due to track reconstruction, muon identification, and trigger requirements. All efficiencies are determined from data using the techniques detailed in refs. [7, 8], where the track reconstruction, muon identification, and muon trigger efficiencies are obtained using tag-and-probe methods on the Z resonance. The tag and probe tracks are required to satisfy the fiducial requirements. The tag must be identified as a muon and be consistent with triggering the event, while the probe is defined so that it is unbiased by the requirement for which the efficiency is being measured. The efficiency is studied as a function of several variables, which describe both the muon kinematics and the detector occupancy. In this analysis the efficiency as a function of muon η is used. The efficiency in each bin of η is defined as the fraction of tag-and-probe candidate events where the probe satisfies a track reconstruction, identification or trigger requirement.

The tracking efficiency is determined using probe tracks that are reconstructed by combining hits from the muon stations and the large-area silicon-strip detector. The efficiency depends on η and varies between 89.5% and 98.5% with uncertainties between 0.4% and 1.9%.

The muon identification efficiency is determined using probe tracks that are reconstructed without using the muon system. The efficiency depends on η and varies between 91.3% and 99.2% with uncertainties between 0.1% and 0.9%.

The single-muon trigger efficiency is determined using reconstructed muons as probes. The efficiency depends on η and varies between 71.6% and 82.0% with uncertainties between 0.5% and 1.2%. Since only one muon candidate is required for the event to pass the trigger requirements, the overall trigger efficiency for the analysis is about 95%.

The efficiency to reconstruct any given event is taken to be the product of the three individual efficiencies and determined on an event-by-event basis as a function of muon η,

$$\varepsilon(\mu^+, \mu^-) = \varepsilon_{\text{trk}}^{\mu^+} \cdot \varepsilon_{\text{trk}}^{\mu^-} \cdot \varepsilon_{\text{id}}^{\mu^+} \cdot \varepsilon_{\text{id}}^{\mu^-} \cdot \left(\varepsilon_{\text{trg}}^{\mu^+} + \varepsilon_{\text{trg}}^{\mu^-} - \varepsilon_{\text{trg}}^{\mu^+} \cdot \varepsilon_{\text{trg}}^{\mu^-} \right). \tag{4.3}$$

In equation (4.3), the efficiency ε is written explicitly in terms of the muon tracking (ε_{trk}), identification (ε_{id}) and trigger (ε_{trg}) efficiencies. The average reconstruction efficiency for the analysis is about 85%. Effects that correlate the efficiency of the two muons are considered, but these are negligible at the current level of precision.

4.2 GEC efficiency

The GEC efficiency is the efficiency of the SPD multiplicity limit at 600 hits in the muon trigger. This efficiency is evaluated from data using two independent methods. The first exploits the fact that the SPD multiplicities of single pp interactions are always below the 600 hit threshold. The expected SPD multiplicity distribution of signal events is constructed by adding the multiplicities of signal events in single pp interactions to the multiplicities of randomly triggered events, as in ref. [7]. The convolution of the distributions extends to values above 600 hits, and the fraction of events that the trigger rejects can be determined. The second method consists of fitting the SPD multiplicity distribution and extrapolating the fit function to determine the fraction of events that are rejected, as in ref. [8]. Both methods give consistent results and $\varepsilon_{\text{GEC}} = (94.0 \pm 0.2)\%$ is used in this analysis. The central value is the estimate from the first method, while the difference between the two estimates contributes to the uncertainty. This efficiency depends linearly on y_Z with about 2% variation across the full range. A weaker dependence on both the $p_{T,Z}$ and ϕ_Z^* is also observed. Corrections for these effects are made.

4.3 Final-state radiation

The FSR correction is taken to be the mean of the corrections calculated with HERWIG++ [63] and PYTHIA8 [25]. The corrections are tabulated in appendix A and are on average about 2.5%.

4.4 Unfolding detector response

To correct for detector resolution effects, an unfolding is performed (matrix U of equation (4.1)) using LHCb simulation and the ROOUNFOLD [64] software package. The momentum resolution in the simulation is calibrated to the data. The data are then unfolded using the iterative Bayesian approach proposed in ref. [65]. Other unfolding techniques [66, 67] give similar results. Additionally, all unfolding methods are tested for model dependence using underlying distributions from leading order PYTHIA [24, 25], leading order HERWIG++ [63], as well as NLO POWHEG [41, 68, 69] showered with both PYTHIA

Source	Uncertainty (%)
Statistical	0.39
Trigger efficiency	0.07
Identification efficiency	0.23
Tracking efficiency	0.53
FSR	0.11
Purity	0.22
GEC efficiency	0.26
Systematic	0.68
Beam energy	1.25
Luminosity	1.72
Total	2.27

Table 1. Contributions to the relative uncertainty on the total Z boson cross-section.

and HERWIG using the POWHEG matching scheme. The correction is on average about 2% as a function of $p_{T,Z}$, while it is significantly less as a function of ϕ_Z^*. Only the $p_{T,Z}$ and ϕ_Z^* distributions are unfolded. Since y_Z is well measured, no unfolding is performed and U is the identity matrix in this case.

4.5 Systematic uncertainties

Sources of systematic uncertainty and their effect on the total cross-section measurement are summarised in table 1.[2] The measured cross-sections as a function of $p_{T,Z}$ and ϕ_Z^* have additional systematic uncertainties due to unfolding.

The systematic uncertainty associated with the trigger, identification and tracking efficiencies is determined by re-evaluating all cross-sections with the values of the individual efficiencies increased or decreased by one standard deviation. The full covariance matrix of the differential cross-section measurements is evaluated in this way for each source of uncertainty separately. The covariance matrices for each source are added and the diagonal elements of the result determine the total systematic uncertainty due to reconstruction efficiencies. These vary between 0.5 and 2.0% on the differential cross-section measurements.

The systematic uncertainty on the FSR correction is the quadratic sum of two components. The first is due to the statistical precision of the PYTHIA and HERWIG++ estimates and the second is half of the difference between their central values. The latter dominates, with the uncertainties on the differential cross-sections varying between 0.3 and 3%.

The systematic uncertainty on the purity is determined from the number of candidate and background events. In addition, an uncertainty based on the assumption that the purity is the same for all variables and bins of the analysis is evaluated by comparing to

---

[2]Many of the systematic uncertainties quoted here have a statistical component. The statistical uncertainty quoted on the measurement is due to the number of observed Z candidates. In the case of unfolded measurements, the statistical uncertainty is provided by the covariance matrix returned by ROOUNFOLD.

cross-section measurements using a binned purity, rather than a global one. The total uncertainties on the differential cross-section measurements due to variations in purity are typically less than 1%.

The GEC efficiency is determined in each bin of y_Z, $p_{T,Z}$ and ϕ_Z^*. The systematic uncertainty is the sum in quadrature of a component due to the available sample size in each bin and a component due to the 0.2% uncertainty on the integrated number, as determined in section 4.2. This varies between 0.4 and 4% across the differential measurements.

The systematic uncertainty due to unfolding is estimated by the differences between the differential cross-sections using Bayesian and matrix inversion unfolding techniques. The typical size is 1.5%.

The measurement is specified at centre-of-mass energy $\sqrt{s} = 7$ TeV. The beam energy, and consequently the centre-of-mass energy, is known to 0.65% [70]. The sensitivity of the cross-section to the centre-of-mass energy is studied using DYNNLO [71] and a systematic uncertainty of 1.25% is assigned.

5   Results

5.1 Z boson production cross-section

The measured rapidity distribution as shown in figure 2 is compared to the prediction from FEWZ [30, 31] with six different PDF sets. To compare the shapes of the differential cross-sections, measurements and predictions are normalised to the total fiducial cross-section. The normalised differential cross-sections are shown in figures 2, 3 and 4. The measurements are compared to the predictions from RESBOS [38–40] and POWHEG [41] where events are interfaced with a parton shower that is simulated using HERWIG [42, 43]. The $p_{T,Z}$ and ϕ_Z^* distributions are well described by RESBOS and POWHEG, with the central values overestimating the data slightly at low ϕ_Z^* and underestimating slightly at high ϕ_Z^*. Comparisons to MC@NLO + HERWIRI and MC@NLO + HERWIG are shown in figures 5 and 6. Here HERWIG is configured with the root mean-square-deviation of the intrinsic k_T distribution set to 0 GeV/c in one instance and 2.2 GeV/c in another. The predictions straddle the measurement at low $p_{T,Z}$ and ϕ_Z^*. The high $p_{T,Z}$ and ϕ_Z^* tails are underestimated.

The total inclusive cross-section for $Z \rightarrow \mu^+\mu^-$ production for muons with $p_T > 20$ GeV/c in the pseudorapidity region $2.0 < \eta < 4.5$ and the dimuon invariant mass range $60 < M_{\mu^+\mu^-} < 120$ GeV/c^2 is measured to be

$$\sigma_{Z\rightarrow\mu^+\mu^-} = (76.0 \pm 0.3 \pm 0.5 \pm 1.0 \pm 1.3)\,\text{pb},$$

where the first uncertainty is statistical, the second systematic, the third is due to the beam energy and the fourth is due to the luminosity. The upper plot of figure 7 shows agreement between this measurement and NNLO predictions given by FEWZ configured with various PDF sets. The measurement also agrees with the measurements of the Z boson production cross-section performed in the electron [8] and tau lepton [9] channels but with a significantly smaller uncertainty. All binned cross-sections are detailed in tables 3, 4 and 5 of appendix A. The degree of correlation between these measurements is given in tables 9, 10 and 11.

5.2 Ratios of electroweak boson production cross-sections

The cross-section ratios are defined for muons with $p_T > 20\,\text{GeV}/c$, $2.0 < \eta < 4.5$ and, in the case of the Z boson cross-section, a dimuon invariant mass between 60 and $120\,\text{GeV}/c^2$. The ratio of W boson to Z boson production is defined as

$$R_{WZ} = \frac{\sigma_{W^+ \to \mu^+ \nu_\mu} + \sigma_{W^- \to \mu^- \bar{\nu}_\mu}}{\sigma_{Z \to \mu^+ \mu^-}}. \tag{5.1}$$

The separate ratios of W^+ and W^- to Z boson production cross-sections are defined as

$$R_{W^\pm Z} = \frac{\sigma_{W^\pm \to \mu^\pm \nu_\mu}}{\sigma_{Z \to \mu^+ \mu^-}}, \tag{5.2}$$

while the W boson cross-section ratio is defined as

$$R_W = \frac{\sigma_{W^+ \to \mu^+ \nu_\mu}}{\sigma_{W^- \to \mu^- \bar{\nu}_\mu}}. \tag{5.3}$$

Many sources of systematic uncertainty cancel or are reduced in the ratios. As the data sets are identical, the largest single source of uncertainty on the individual cross-sections, due to the luminosity determination, is removed. The trigger used to select both samples is identical and most of the uncertainty on the determination of the trigger efficiency cancels. In particular, the GEC is common to both the W and Z boson analyses and it is expected that the size of the efficiency correction is similar for W and Z events. Cross-checks in data and simulation support this assumption with a precision of approximately 0.3%, which is included as a systematic uncertainty. The GEC efficiency was determined for the previous W boson measurement [10] to be $(95.9 \pm 1.1)\%$, whereas an improved precision of $(94.0 \pm 0.2)\%$ is obtained in the current analysis. Consequently, the W boson cross-section results are updated to benefit from the more precise value. These results are listed in tables 6, 7 and 8 of appendix A, along with the muon charge ratios and asymmetries, and supersede those in ref. [10]. The uncertainties on the tracking and muon identification partially cancel in the ratios of W and Z bosons. The uncertainty on the $W^+(W^-)$ cross-section due to beam energy is 1.06(0.91)% and most of this uncertainty also cancels in the ratios. The uncertainties on the purities of the W and Z boson selections are uncorrelated. The FSR uncertainties are taken to be uncorrelated. The sources of uncertainty contributing to the determination of the ratios are summarised in table 2.

The dominant uncertainties on the ratios are due to the purity and the size of the sample. The correlation coefficients used in the uncertainty calculations are given in tables 9, 12 and 13.

The updated W^+ boson cross-section is

$$\sigma_{W^+ \to \mu^+ \nu_\mu} = (878.0 \pm 2.1 \pm 6.7 \pm 9.3 \pm 15.0)\ \text{pb},$$

where the uncertainties are due to the sample size, systematic effects, the beam energy and the luminosity determination. The updated W^- boson cross-section is

$$\sigma_{W^- \to \mu^- \bar{\nu}_\mu} = (689.5 \pm 2.0 \pm 5.3 \pm 6.3 \pm 11.8)\ \text{pb}.$$

Source	Uncertainty (%)			
	R_{WZ}	R_{W^+Z}	R_{W^-Z}	R_W
Statistical	0.45	0.48	0.50	0.38
Trigger efficiency	0.15	0.16	0.13	0.07
Identification efficiency	0.12	0.12	0.12	0.03
Tracking efficiency	0.24	0.23	0.26	0.08
FSR	0.16	0.21	0.17	0.21
Purity	0.41	0.49	0.55	0.62
GEC efficiency	0.27	0.28	0.29	0.18
Systematic	0.60	0.67	0.72	0.69
Beam energy	0.26	0.19	0.34	0.15
Total	0.79	0.85	0.94	0.80

Table 2. Contributions to the relative uncertainty on the electroweak boson cross-section ratios.

These measurements are in good agreement with the predictions of NNLO pQCD, as shown in figure 7. Using the Z boson cross-section from section 5.1, electroweak boson cross-section measurements and theoretical predictions, with different parameterisations of the PDFs, are compared in figure 8, with contours corresponding to the 68.3% confidence level.

The W to Z boson cross-section ratio is measured as

$$R_{WZ} = 20.63 \pm 0.09 \pm 0.12 \pm 0.05,$$

where the first uncertainty is statistical, the second is systematic and the third is due to the beam energy. The charged W to Z boson cross-section ratios are measured as

$$R_{W^+Z} = 11.56 \pm 0.06 \pm 0.08 \pm 0.02,$$
$$R_{W^-Z} = 9.07 \pm 0.05 \pm 0.07 \pm 0.03,$$

while the W boson cross-section ratio is measured as

$$R_W = 1.274 \pm 0.005 \pm 0.009 \pm 0.002.$$

These measurements, as well as their predictions, are displayed in figure 9. For R_{WZ} and R_{W^+Z}, the data are well described by HERA1.5 and JR09, while the values from CT10, MSTW08, NNPDF3.0 and ABM12 are larger than those measured. All PDF sets show good agreement for R_{W^-Z}. As previously reported [10], all PDF sets except ABM12 show good agreement for R_W. The R_{WZ} and R_W ratios are measured with a fractional uncertainty of 0.8%, which is similar both to the precision due to the PDFs on the individual theoretical predictions and to the spread between the predictions. Considering the spread in the different predictions, the experimental measurements are in good agreement with SM predictions and can be used to improve the determination of the PDFs.
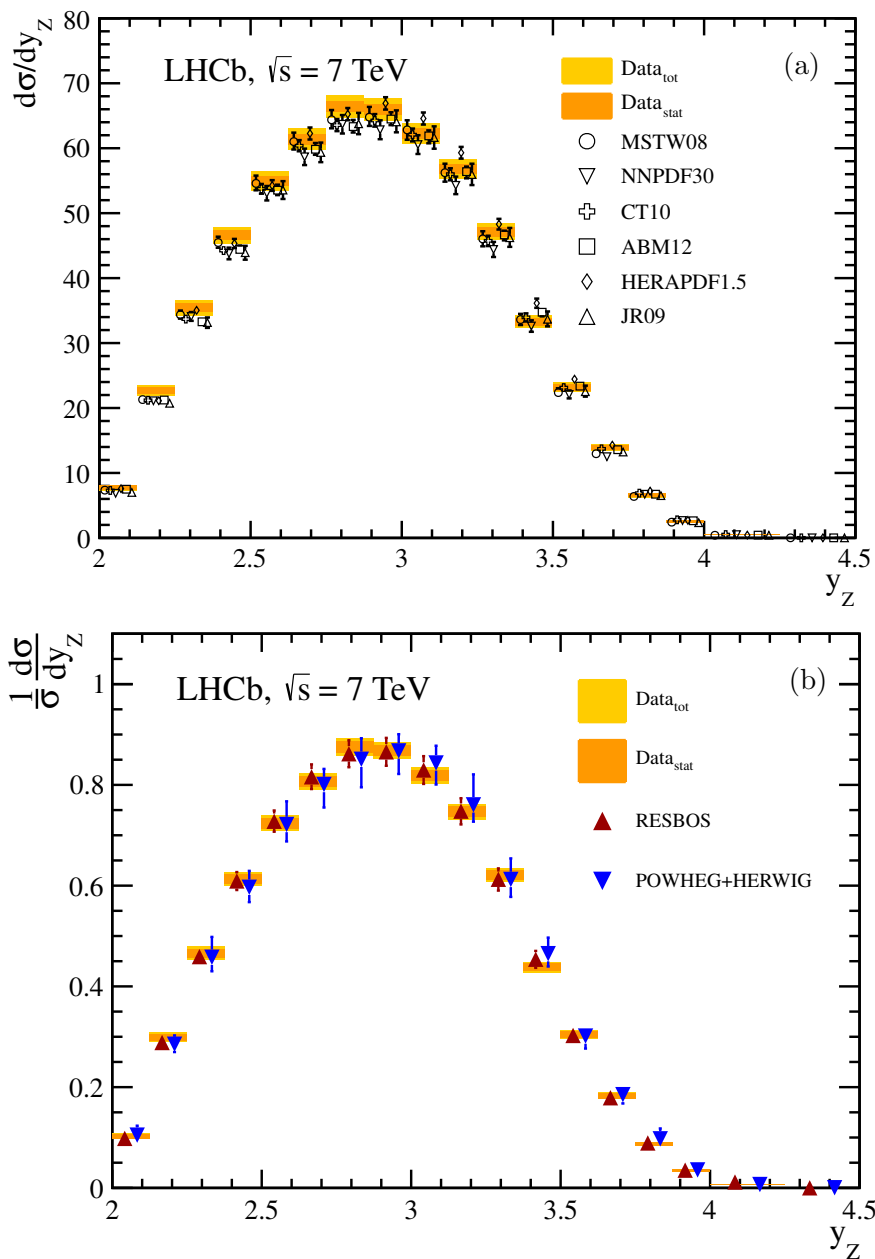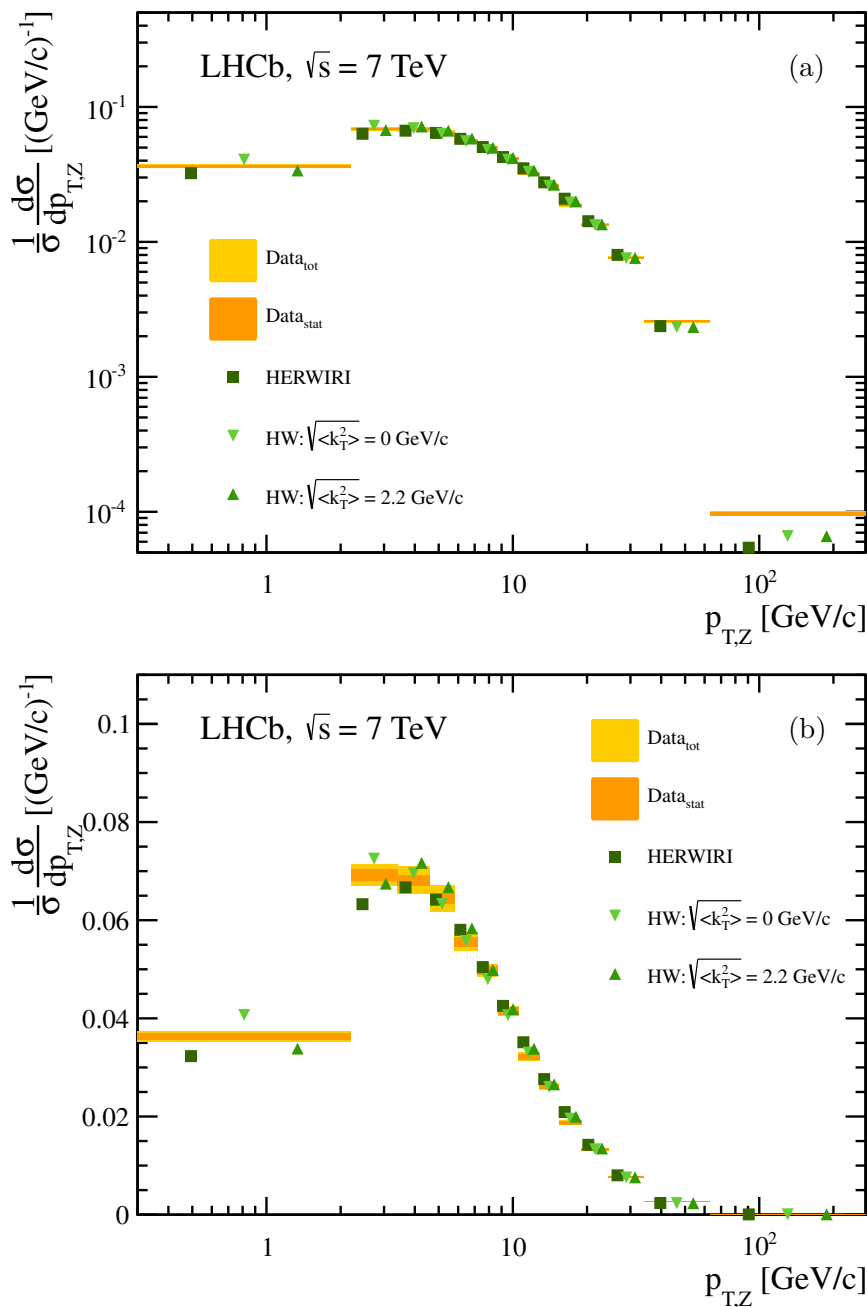
Figure 2. (a) Differential cross-section as a function of y_Z compared with the prediction of Fewz configured with various PDF sets. Different predictions are displaced horizontally for visibility. (b) Normalised differential cross-section as a function of y_Z compared to the predictions of ResBos and Powheg + Herwig. The shaded (yellow) bands indicate the statistical and total uncertainties on the measurements, which are symmetric about the central value.
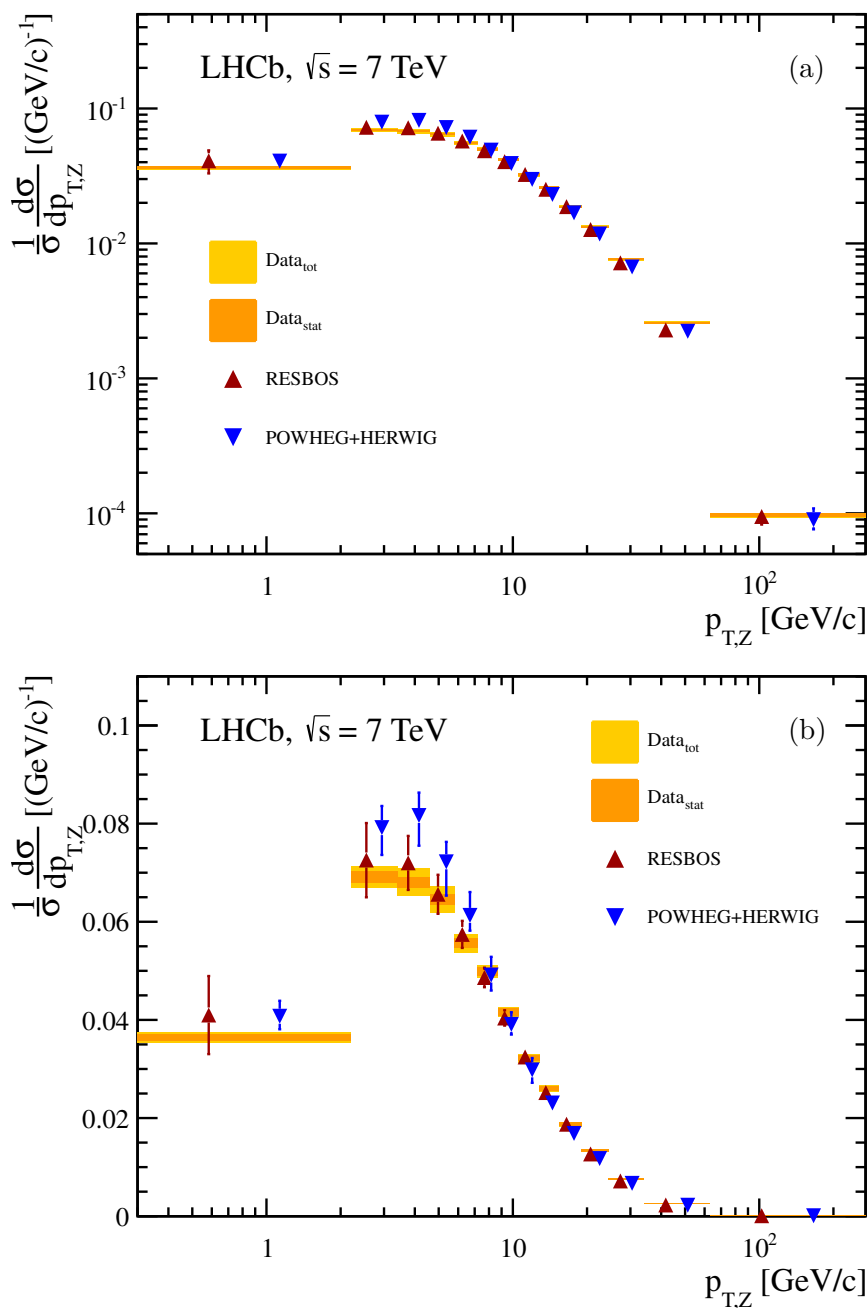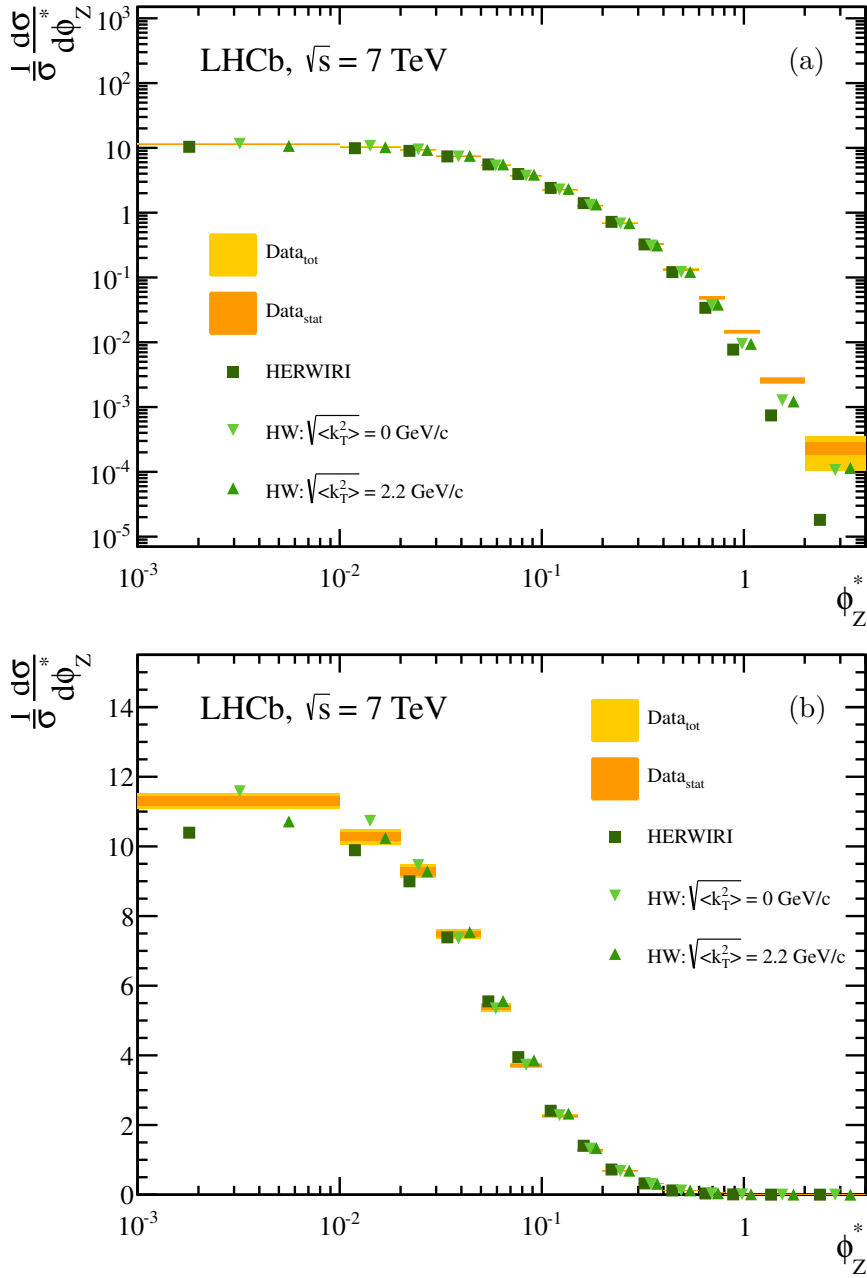
Figure 3. Normalised differential cross-section as a function of $p_{T,Z}$ on (a) logarithmic and (b) linear scales. The shaded (yellow) bands indicate the statistical and total uncertainties on the measurements, which are symmetric about the central value. The measurements are compared to the predictions of RESBOS and POWHEG + HERWIG.
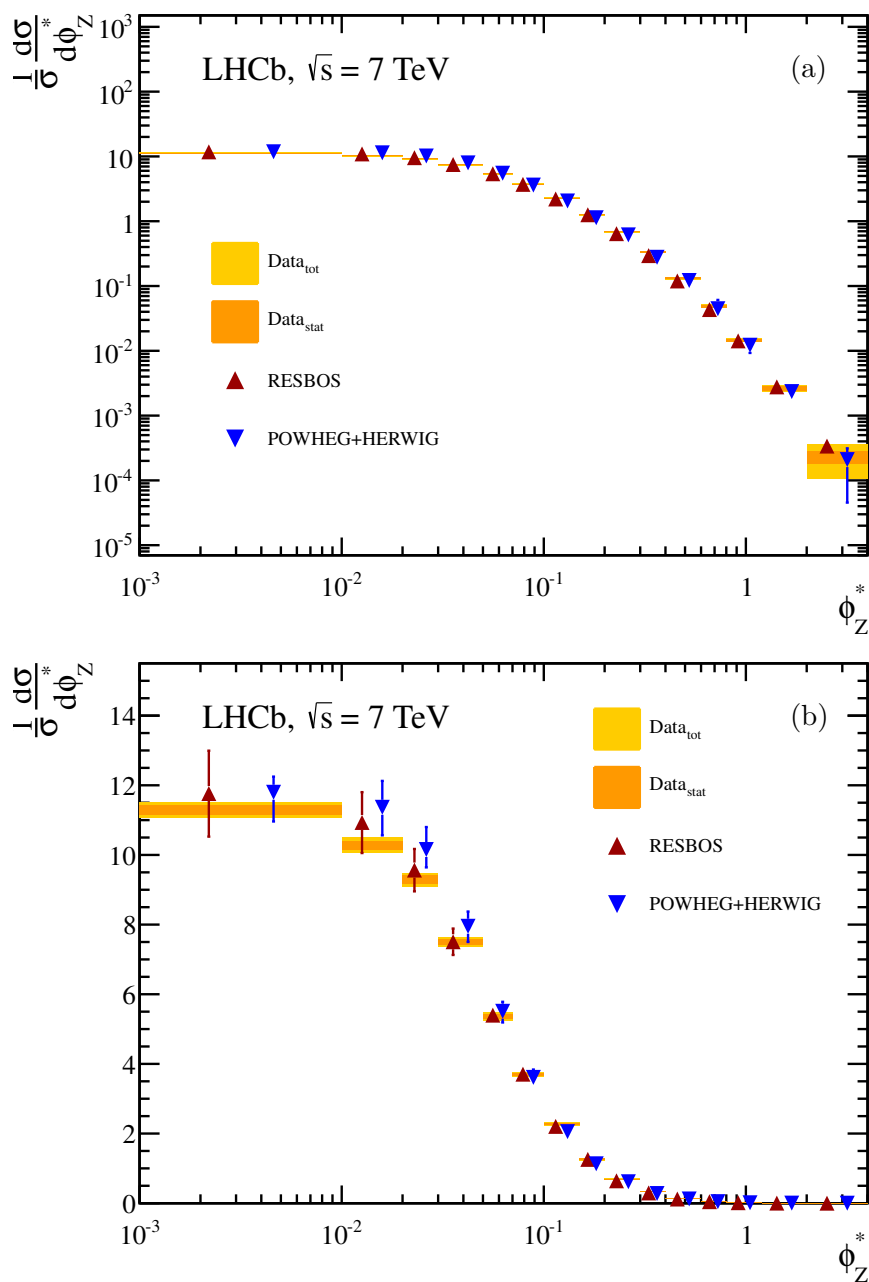
Figure 4. Normalised differential cross-section as a function of ϕ_Z^* on (a) logarithmic and (b) linear scales. The shaded (yellow) bands indicate the statistical and total uncertainties on the measurements, which are symmetric about the central value. The measurements are compared to the predictions of RESBOS and POWHEG + HERWIG.

Figure 5. Normalised differential cross-section as a function of $p_{T,Z}$ on (a) logarithmic and (b) linear scales. The shaded (yellow) bands indicate the statistical and total uncertainties on the measurements, which are symmetric about the central value. The measurements are compared to MC@NLO + Herwig (HW) and MC@NLO + Herwiri (HERWIRI). Herwig is configured with two choices of the root mean-square-deviation of the intrinsic k_T distribution, 0 and 2.2 GeV/c.
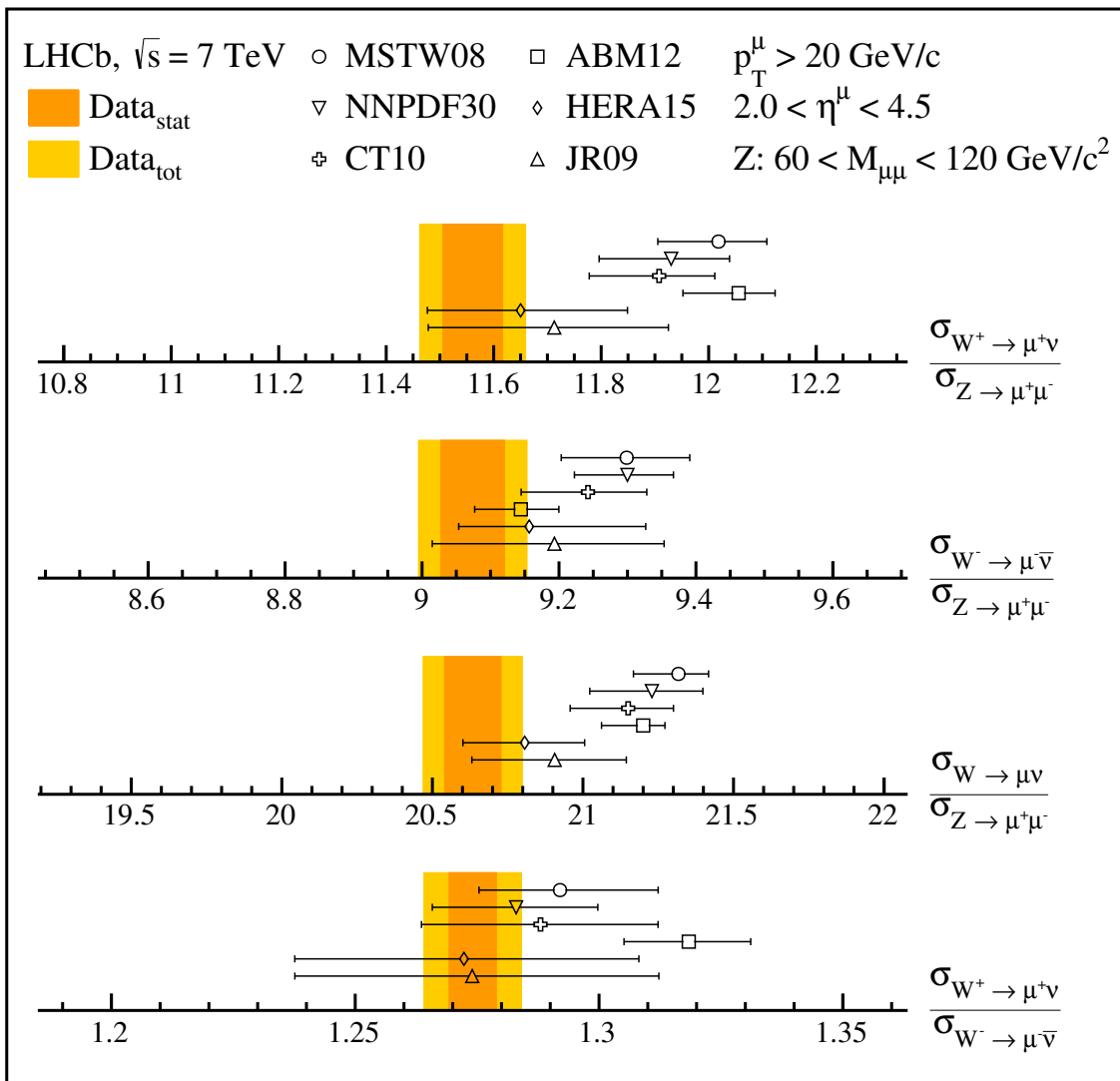
Figure 6. Normalised differential cross-section as a function of ϕ_Z^* on (a) logarithmic and (b) linear scales. The shaded (yellow) bands indicate the statistical and total uncertainties on the measurements, which are symmetric about the central value. The measurements are compared to MC@NLO + HERWIG (HW) and MC@NLO + HERWIRI (HERWIRI). HERWIG is configured with two choices of the root mean-square-deviation of the intrinsic k_T distribution, 0 and 2.2 GeV/c.
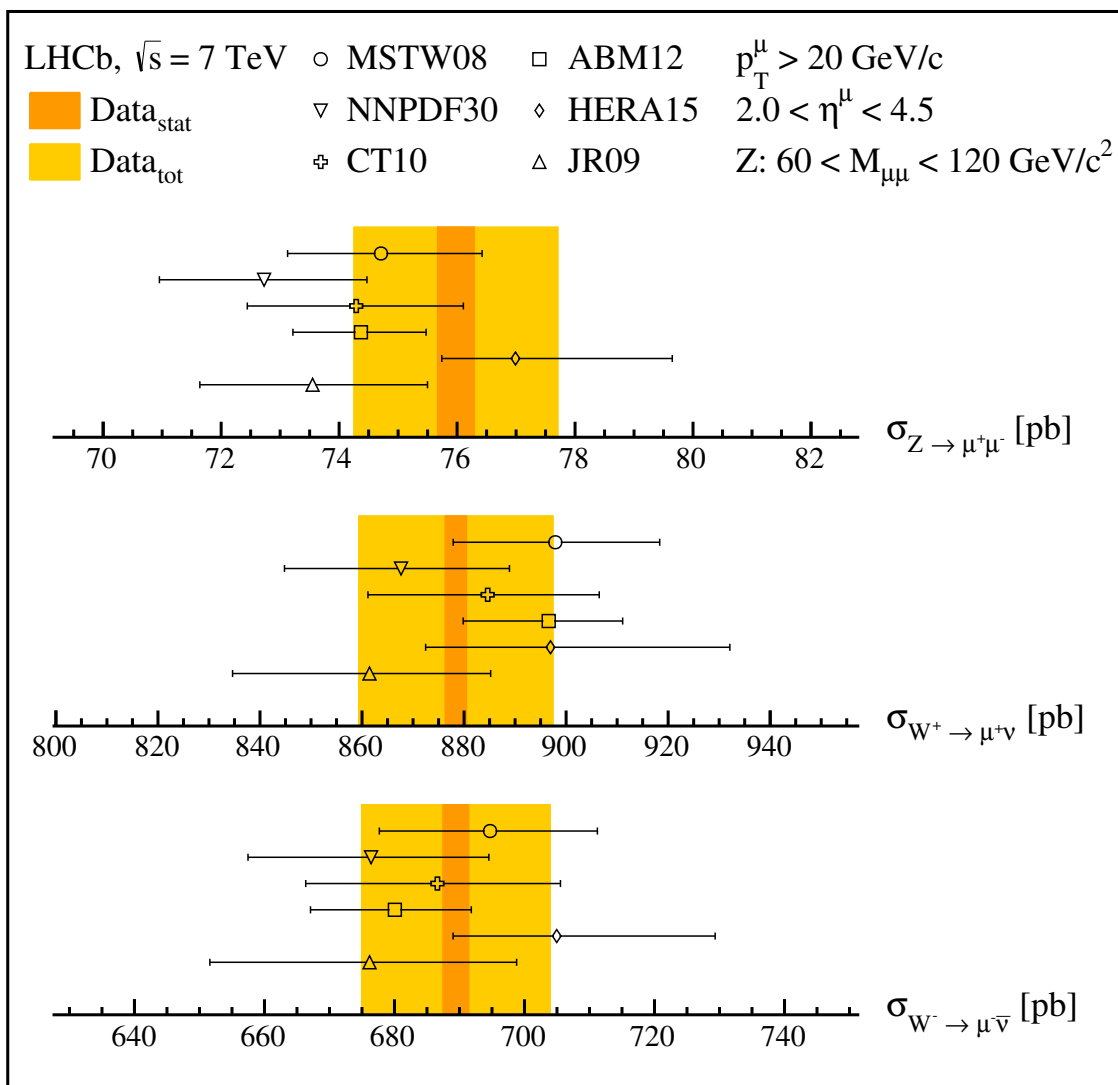
Figure 7. LHCb measurements of electroweak boson production cross-sections compared to NNLO pQCD as implemented by the Fewz generator using various PDF sets. The shaded (yellow) bands indicate the statistical and total uncertainties on the measurements, which are symmetric about the central value.
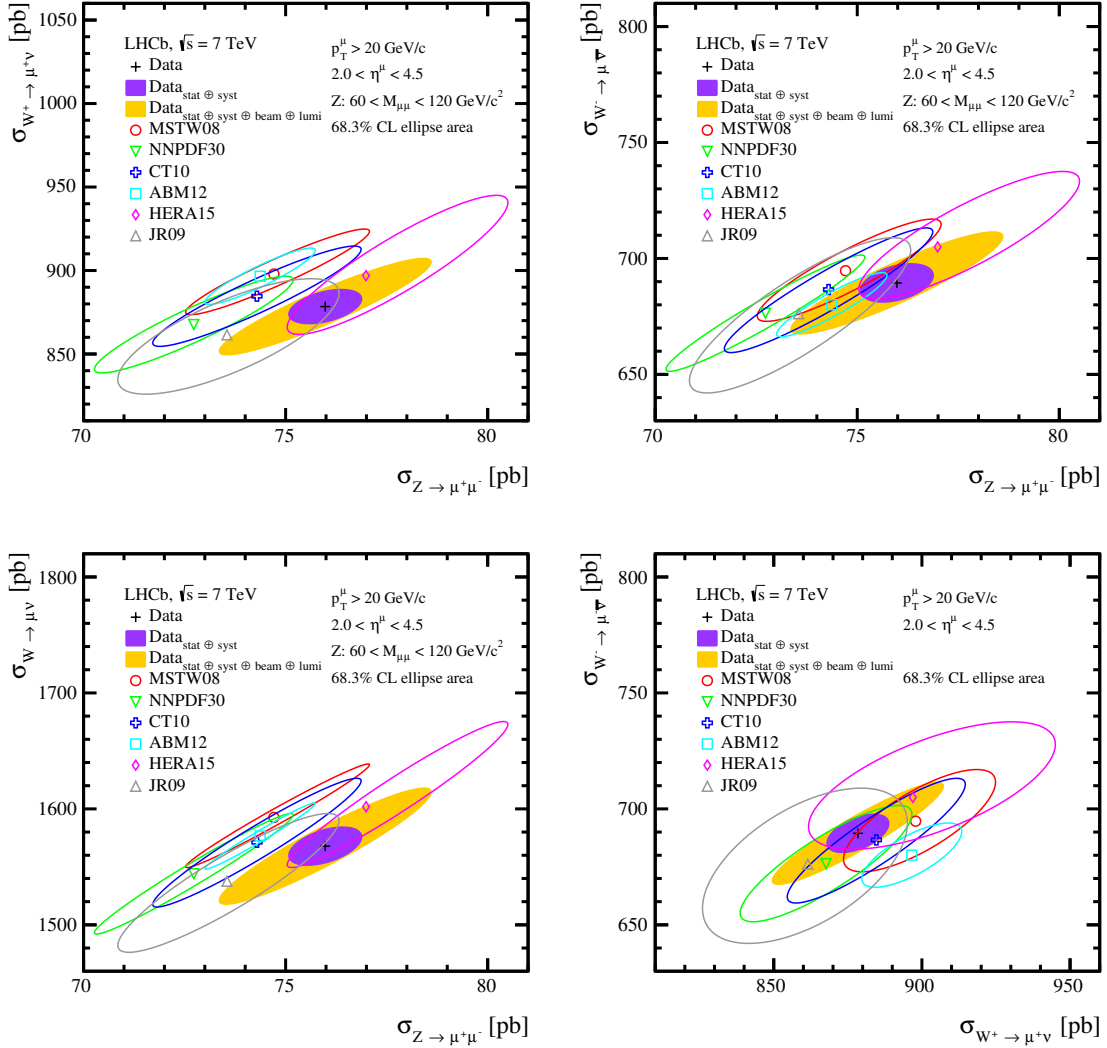
Figure 8. Two dimensional plots of electroweak boson cross-sections compared to NNLO predictions for various parameterisations of the PDFs. The outer, shaded (yellow) ellipse corresponds to the total uncertainty on the measurements. The inner, shaded (purple) ellipse excludes the beam energy and luminosity uncertainties. The uncertainty on the theoretical predictions corresponds to the PDF uncertainty only. All ellipses correspond to uncertainties at 68.3% confidence level.

Figure 9. Ratios of electroweak boson production R_{W^+Z}, R_{W^-Z}, R_{WZ}, R_W, compared to various theoretical predictions. The shaded (yellow) bands indicate the statistical and total uncertainties on the measurements, which are symmetric about the central value.

6   Conclusions

A measurement of the forward Z boson production cross-section at $\sqrt{s} = 7\,\text{TeV}$ is presented, where the Z bosons are reconstructed in the decay $Z \to \mu^+\mu^-$. The total cross-section in the fiducial range of the selection is in agreement with NNLO pQCD calculations. Normalised differential cross-sections as a function of y_Z, ϕ_Z^* and $p_{T,Z}$ are compared to the predictions of various generators. The increased precision on the determination of the event trigger efficiency motivates a re-evaluation of the recently measured W boson production cross-section. These are presented here and supersede the values given in ref. [10]. Combining the Z boson cross-section with updated W boson cross-sections measured in a similar fiducial volume allows for precision measurements of electroweak boson cross-section ratios. In particular, the W to Z boson ratio is determined with a relative precision of 0.8%. The measured ratios are consistent with SM predictions but are sensitive to the particular choice of PDF. Consequently, these results are expected to provide significant constraints on PDFs.

A Cross-sections

y_Z	σ_Z [pb]	f_{FSR}
$2.000 - 2.125$	$0.969 \pm 0.039 \pm 0.032 \pm 0.012 \pm 0.017$	1.050 ± 0.020
$2.125 - 2.250$	$2.840 \pm 0.063 \pm 0.050 \pm 0.036 \pm 0.049$	1.032 ± 0.008
$2.250 - 2.375$	$4.428 \pm 0.077 \pm 0.078 \pm 0.055 \pm 0.076$	1.027 ± 0.006
$2.375 - 2.500$	$5.823 \pm 0.088 \pm 0.060 \pm 0.073 \pm 0.100$	1.026 ± 0.004
$2.500 - 2.625$	$6.877 \pm 0.095 \pm 0.068 \pm 0.086 \pm 0.118$	1.025 ± 0.004
$2.625 - 2.750$	$7.669 \pm 0.100 \pm 0.069 \pm 0.096 \pm 0.132$	1.026 ± 0.004
$2.750 - 2.875$	$8.306 \pm 0.104 \pm 0.070 \pm 0.104 \pm 0.143$	1.026 ± 0.003
$2.875 - 3.000$	$8.241 \pm 0.103 \pm 0.066 \pm 0.103 \pm 0.142$	1.025 ± 0.003
$3.000 - 3.125$	$7.783 \pm 0.099 \pm 0.059 \pm 0.097 \pm 0.134$	1.026 ± 0.003
$3.125 - 3.250$	$7.094 \pm 0.096 \pm 0.058 \pm 0.089 \pm 0.122$	1.028 ± 0.004
$3.250 - 3.375$	$5.894 \pm 0.087 \pm 0.049 \pm 0.074 \pm 0.101$	1.026 ± 0.004
$3.375 - 3.500$	$4.160 \pm 0.073 \pm 0.041 \pm 0.052 \pm 0.072$	1.027 ± 0.005
$3.500 - 3.625$	$2.896 \pm 0.061 \pm 0.030 \pm 0.036 \pm 0.050$	1.026 ± 0.005
$3.625 - 3.750$	$1.741 \pm 0.047 \pm 0.023 \pm 0.022 \pm 0.030$	1.021 ± 0.007
$3.750 - 3.875$	$0.825 \pm 0.032 \pm 0.014 \pm 0.010 \pm 0.014$	1.025 ± 0.010
$3.875 - 4.000$	$0.321 \pm 0.020 \pm 0.008 \pm 0.004 \pm 0.006$	1.011 ± 0.015
$4.000 - 4.250$	$0.115 \pm 0.013 \pm 0.006 \pm 0.001 \pm 0.002$	1.018 ± 0.033
$4.250 - 4.500$	—	—

Table 3. Inclusive differential cross-sections for Z boson production as a function of y_Z. Uncertainties are due to the sample size, systematic effects, the beam energy and the luminosity. No candidates are observed in the 4.250–4.500 bin.

$p_{T,Z}[\,\mathrm{GeV}/c]$	σ_Z [pb]	f_{FSR}
0.0 − 2.2	6.454 ± 0.105± 0.129 ± 0.081 ± 0.111	1.090±0.006
2.2 − 3.4	6.520 ± 0.106± 0.150 ± 0.081 ± 0.112	1.080±0.004
3.4 − 4.6	6.209 ± 0.102± 0.221 ± 0.078 ± 0.107	1.063±0.004
4.6 − 5.8	5.868 ± 0.099± 0.208 ± 0.073 ± 0.101	1.049±0.004
5.8 − 7.2	5.749 ± 0.098± 0.154 ± 0.072 ± 0.099	1.034±0.004
7.2 − 8.7	5.607 ± 0.098± 0.083 ± 0.070 ± 0.096	1.021±0.004
8.7 − 10.5	5.637 ± 0.098± 0.054 ± 0.070 ± 0.097	1.002±0.004
10.5 − 12.8	5.524 ± 0.096± 0.081 ± 0.069 ± 0.095	0.996±0.004
12.8 − 15.4	5.158 ± 0.092± 0.067 ± 0.064 ± 0.089	0.984±0.005
15.4 − 19.0	4.963 ± 0.087± 0.053 ± 0.062 ± 0.085	0.978±0.005
19.0 − 24.5	5.517 ± 0.088± 0.055 ± 0.069 ± 0.095	0.985±0.004
24.5 − 34.0	5.465 ± 0.085± 0.067 ± 0.068 ± 0.094	1.013±0.004
34.0 − 63.0	5.789 ± 0.085± 0.076 ± 0.072 ± 0.100	1.038±0.004
63.0 − 270.0	1.516 ± 0.043± 0.044 ± 0.019 ± 0.026	1.060±0.007

Table 4. Inclusive differential cross-sections for Z boson production as a function of $p_{T,Z}$. Uncertainties are due to the sample size, systematic effects, the beam energy and the luminosity.

ϕ_Z^*	σ_Z [pb]	f_{FSR}
0.00 − 0.01	8.549 ± 0.099 ± 0.088 ± 0.107 ± 0.147	1.034±0.004
0.01 − 0.02	7.805 ± 0.096 ± 0.106 ± 0.098 ± 0.134	1.035±0.003
0.02 − 0.03	7.051 ± 0.091 ± 0.083 ± 0.088 ± 0.121	1.034±0.004
0.03 − 0.05	11.362 ± 0.114 ± 0.108 ± 0.142 ± 0.195	1.029±0.003
0.05 − 0.07	8.124 ± 0.097 ± 0.120 ± 0.102 ± 0.140	1.026±0.003
0.07 − 0.10	8.436 ± 0.097 ± 0.074 ± 0.105 ± 0.145	1.021±0.003
0.10 − 0.15	8.611 ± 0.098 ± 0.131 ± 0.108 ± 0.148	1.020±0.003
0.15 − 0.20	4.819 ± 0.073 ± 0.092 ± 0.060 ± 0.083	1.018±0.004
0.20 − 0.30	5.206 ± 0.076 ± 0.058 ± 0.065 ± 0.090	1.019±0.004
0.30 − 0.40	2.541 ± 0.054 ± 0.051 ± 0.032 ± 0.044	1.022±0.006
0.40 − 0.60	2.018 ± 0.048 ± 0.060 ± 0.025 ± 0.035	1.024±0.007
0.60 − 0.80	0.755 ± 0.029 ± 0.035 ± 0.009 ± 0.013	1.029±0.011
0.80 − 1.20	0.457 ± 0.023 ± 0.018 ± 0.006 ± 0.008	1.025±0.014
1.20 − 2.00	0.166 ± 0.014 ± 0.011 ± 0.002 ± 0.003	1.030±0.023
2.00 − 4.00	0.045 ± 0.008 ± 0.017 ± 0.001 ± 0.001	1.031±0.041

Table 5. Inclusive differential cross-sections for Z boson production as a function of ϕ_Z^*. Uncertainties are due to the sample size, systematic effects, the beam energy and the luminosity.

η^μ	σ_{W^+} [pb]	$f_{\mathrm{FSR}}^{W^+}$	σ_{W^-} [pb]	$f_{\mathrm{FSR}}^{W^-}$
$2.00 - 2.25$	$192.2 \pm 1.2 \pm 3.5 \pm 2.0 \pm 3.3$	1.016 ± 0.004	$111.1 \pm 0.9 \pm 2.1 \pm 1.0 \pm 1.9$	1.019 ± 0.003
$2.25 - 2.50$	$178.8 \pm 0.9 \pm 3.1 \pm 1.9 \pm 3.1$	1.018 ± 0.004	$104.9 \pm 0.7 \pm 1.9 \pm 1.0 \pm 1.8$	1.015 ± 0.003
$2.50 - 2.75$	$154.3 \pm 0.8 \pm 2.1 \pm 1.6 \pm 2.6$	1.025 ± 0.005	$96.1 \pm 0.7 \pm 1.3 \pm 0.9 \pm 1.6$	1.010 ± 0.003
$2.75 - 3.00$	$122.8 \pm 0.7 \pm 1.6 \pm 1.3 \pm 2.1$	1.015 ± 0.004	$88.4 \pm 0.7 \pm 1.5 \pm 0.8 \pm 1.5$	1.007 ± 0.002
$3.00 - 3.25$	$94.3 \pm 0.6 \pm 1.3 \pm 1.0 \pm 1.6$	1.021 ± 0.005	$80.6 \pm 0.6 \pm 1.4 \pm 0.7 \pm 1.4$	1.009 ± 0.003
$3.25 - 3.50$	$61.6 \pm 0.5 \pm 0.9 \pm 0.7 \pm 1.1$	1.015 ± 0.005	$68.6 \pm 0.6 \pm 1.5 \pm 0.6 \pm 1.2$	1.017 ± 0.005
$3.50 - 4.00$	$60.0 \pm 0.5 \pm 0.7 \pm 0.6 \pm 1.0$	1.024 ± 0.005	$95.9 \pm 0.7 \pm 1.2 \pm 0.9 \pm 1.6$	1.012 ± 0.005
$4.00 - 4.50$	$14.3 \pm 0.4 \pm 0.4 \pm 0.2 \pm 0.2$	1.021 ± 0.005	$43.8 \pm 0.8 \pm 1.2 \pm 0.4 \pm 0.7$	1.000 ± 0.000

Table 6. Inclusive differential cross-sections for W^+ (left) and W^- (right) boson production as a function of muon η. Uncertainties are due to the sample size, systematic effects, the beam energy and the luminosity. These supersede the results in ref. [10].

η^μ	R_W
$2.00 - 2.25$	$1.730 \pm 0.018 \pm 0.030 \pm 0.003$
$2.25 - 2.50$	$1.706 \pm 0.015 \pm 0.040 \pm 0.003$
$2.50 - 2.75$	$1.606 \pm 0.014 \pm 0.021 \pm 0.002$
$2.75 - 3.00$	$1.388 \pm 0.013 \pm 0.024 \pm 0.002$
$3.00 - 3.25$	$1.169 \pm 0.012 \pm 0.021 \pm 0.002$
$3.25 - 3.50$	$0.898 \pm 0.010 \pm 0.025 \pm 0.001$
$3.50 - 4.00$	$0.626 \pm 0.007 \pm 0.006 \pm 0.001$
$4.00 - 4.50$	$0.328 \pm 0.011 \pm 0.011 \pm 0.000$

Table 7. W^+ to W^- boson production cross-section ratios as a function of muon η. Uncertainties are due to the sample size, systematic effects and the beam energy. These supersede the results in ref. [10].

η^μ	A_μ [%]
$2.00 - 2.25$	$26.74 \pm 0.48 \pm 0.82 \pm 0.07$
$2.25 - 2.50$	$26.08 \pm 0.41 \pm 1.09 \pm 0.07$
$2.50 - 2.75$	$23.25 \pm 0.42 \pm 0.60 \pm 0.07$
$2.75 - 3.00$	$16.26 \pm 0.46 \pm 0.84 \pm 0.07$
$3.00 - 3.25$	$7.81 \pm 0.50 \pm 0.90 \pm 0.08$
$3.25 - 3.50$	$-5.37 \pm 0.57 \pm 1.35 \pm 0.08$
$3.50 - 4.00$	$-23.04 \pm 0.52 \pm 0.49 \pm 0.07$
$4.00 - 4.50$	$-50.65 \pm 1.22 \pm 1.30 \pm 0.06$

Table 8. Lepton charge asymmetries as a function of muon η. Uncertainties are due to the sample size, systematic effects and the beam energy. These supersede the results in ref. [10].

B Correlation matrices

y_Z	2–2.125	2.125–2.25	2.25–2.375	2.375–2.5	2.5–2.625	2.625–2.75	2.75–2.875	2.875–3	3–3.125	3.125–3.25	3.25–3.375	3.375–3.5	3.5–3.625	3.625–3.75	3.75–3.875	3.875–4	4–4.25	4.25–4.5
2–2.125	1																	
2.125–2.25	0.18	1																
2.25–2.375	0.14	0.19	1															
2.375–2.5	0.14	0.19	0.18	1														
2.5–2.625	0.13	0.18	0.16	0.19	1													
2.625–2.75	0.12	0.16	0.15	0.18	0.18	1												
2.75–2.875	0.11	0.15	0.14	0.17	0.17	0.18	1											
2.875–3	0.10	0.13	0.13	0.16	0.16	0.17	0.17	1										
3–3.125	0.09	0.12	0.12	0.14	0.15	0.15	0.16	0.16	1									
3.125–3.25	0.08	0.1	0.10	0.12	0.13	0.14	0.14	0.14	0.14	1								
3.25–3.375	0.06	0.08	0.08	0.11	0.11	0.12	0.12	0.13	0.13	0.13	1							
3.375–3.5	0.05	0.06	0.06	0.08	0.09	0.09	0.10	0.10	0.11	0.11	0.11	1						
3.5–3.625	0.04	0.05	0.05	0.06	0.07	0.08	0.08	0.09	0.09	0.10	0.10	0.10	1					
3.625–3.75	0.03	0.04	0.03	0.04	0.05	0.06	0.06	0.07	0.07	0.08	0.09	0.08	0.08	1				
3.75–3.875	0.02	0.03	0.02	0.03	0.03	0.04	0.04	0.05	0.05	0.06	0.06	0.06	0.06	0.06	1			
3.875–4	0.02	0.02	0.02	0.02	0.02	0.02	0.02	0.03	0.03	0.04	0.04	0.04	0.04	0.04	0.03	1		
4–4.25	0.01	0.01	0.01	0.01	0.01	0.01	0.01	0.02	0.02	0.02	0.03	0.03	0.03	0.03	0.02	0.02	1	
4.25–4.5	–	–	–	–	–	–	–	–	–	–	–	–	–	–	–	–	–	–

Table 9. Correlation coefficients of differential cross-section measurements as a function of y_Z. The beam energy and luminosity uncertainties, which are fully correlated between cross-section measurements, are excluded.

$p_{T,Z}$ [GeV/c]	0.0–2.2	2.2–3.4	3.4–4.6	4.6–5.8	5.8–7.2	7.2–8.7	8.7–10.5	10.5–12.8	12.8–15.4	15.4–19	19–24.5	24.5–34	34–63	63–270
0.0–2.2	1													
2.2–3.4	-0.01	1												
3.4–4.6	0.00	0.03	1											
4.6–5.8	0.04	0.00	0.02	1										
5.8–7.2	0.05	0.05	0.00	0.03	1									
7.2–8.7	0.07	0.07	0.05	0.00	0.03	1								
8.7–10.5	0.08	0.08	0.06	0.06	0.02	0.02	1							
10.5–12.8	0.07	0.06	0.05	0.05	0.07	0.04	0.00	1						
12.8–15.4	0.07	0.07	0.05	0.05	0.06	0.09	0.07	-0.01	1					
15.4–19	0.08	0.08	0.05	0.06	0.07	0.10	0.12	0.08	-0.01	1				
19–24.5	0.08	0.08	0.06	0.06	0.07	0.10	0.12	0.10	0.10	0.02	1			
24.5–34	0.08	0.07	0.05	0.06	0.07	0.10	0.11	0.09	0.10	0.11	0.05	1		
34–63	0.07	0.06	0.05	0.05	0.06	0.08	0.09	0.08	0.08	0.09	0.10	0.06	1	
63–270	0.20	0.20	0.15	0.15	0.19	0.26	0.30	0.26	0.27	0.30	0.32	0.31	0.30	1

Table 10. Correlation coefficients of differential cross-section measurements as a function of $p_{T,Z}$. The beam energy and luminosity uncertainties, which are fully correlated between cross-section measurements, are excluded.

ϕ_Z^*	0.00–0.01	0.01–0.02	0.02–0.03	0.03–0.05	0.05–0.07	0.07–0.10	0.10–0.15	0.15–0.20	0.20–0.30	0.30–0.40	0.40–0.60	0.60–0.80	0.80–1.20	1.20–2.00	2.00–4.00
0.00–0.01	1														
0.01–0.02	0.14	1													
0.02–0.03	0.16	0.12	1												
0.03–0.05	0.20	0.17	0.17	1											
0.05–0.07	0.15	0.12	0.13	0.16	1										
0.07–0.10	0.19	0.16	0.17	0.21	0.15	1									
0.10–0.15	0.14	0.12	0.13	0.16	0.12	0.15	1								
0.15–0.20	0.11	0.10	0.10	0.13	0.10	0.12	0.09	1							
0.20–0.30	0.15	0.13	0.13	0.17	0.13	0.16	0.13	0.10	1						
0.30–0.40	0.10	0.08	0.09	0.11	0.08	0.10	0.08	0.06	0.08	1					
0.40–0.60	0.07	0.06	0.07	0.08	0.06	0.08	0.06	0.05	0.07	0.04	1				
0.60–0.80	0.05	0.04	0.04	0.05	0.04	0.05	0.04	0.03	0.04	0.03	0.02	1			
0.80–1.20	0.05	0.04	0.04	0.05	0.04	0.05	0.04	0.03	0.04	0.03	0.02	0.01	1		
1.20–2.00	0.02	0.02	0.02	0.03	0.02	0.03	0.02	0.02	0.02	0.01	0.01	0.01	0.00	1	
2.00–4.00	0.005	0.004	0.005	0.006	0.004	0.005	0.004	0.004	0.004	0.002	0.002	0.002	0.002	0.001	1

Table 11. Correlation coefficients of differential cross-section measurements as a function of ϕ_Z^*. The beam energy and luminosity uncertainties, which are fully correlated between cross-section measurements, are excluded.

η^{μ}	2–2.25		2.25–2.5		2.5–2.75		2.75–3		3–3.25		3.25–3.5		3.5–4		4–4.5		
	W^+	W^-	W^+	W^-	W^+	W^-	W^+	W^-	W^+	W^-	W^+	W^-	W^+	W^-	W^+	W^-	
2–2.25	1																W^+
	0.46	1															W^-
2.25–2.5	-0.15	0.34	1														W^+
	0.30	-0.24	0.09	1													W^-
2.5–2.75	-0.03	0.23	0.27	-0.13	1												W^+
	0.24	-0.14	-0.21	0.35	0.41	1											W^-
2.75–3	0.20	-0.07	-0.10	0.25	-0.00	0.21	1										W^+
	-0.19	0.39	0.46	-0.37	0.27	-0.24	0.28	1									W^-
3–3.25	-0.03	0.24	0.28	-0.16	0.20	-0.08	-0.01	0.29	1								W^+
	0.31	-0.23	-0.32	0.46	-0.13	0.35	0.25	-0.37	0.27	1							W^-
3.25–3.5	-0.12	0.29	0.36	-0.27	0.22	-0.17	-0.07	0.40	0.24	-0.27	1						W^+
	0.33	-0.32	-0.41	0.52	-0.19	0.40	0.28	-0.47	-0.21	0.53	-0.07	1					W^-
3.5–4	0.02	0.15	0.18	-0.05	0.15	-0.01	0.04	0.17	0.14	-0.04	0.15	-0.08	1				W^+
	0.21	-0.09	-0.14	0.30	-0.02	0.25	0.19	-0.17	-0.04	0.30	-0.12	0.33	0.45	1			W^-
4–4.5	-0.01	0.13	0.17	-0.08	0.14	-0.05	-0.01	0.15	0.11	-0.07	0.11	-0.12	0.09	0.02	1		W^+
	0.08	0.01	-0.01	0.09	0.03	0.08	0.07	-0.02	0.02	0.10	-0.02	0.09	0.03	0.10	0.11	1	W^-
	W^+	W^-	W^+	W^-	W^+	W^-	W^+	W^-	W^+	W^-	W^+	W^-	W^+	W^-	W^+	W^-	

Table 12. Correlation coefficients between differential cross-section measurements as a function of W boson muon η. The beam energy and luminosity uncertainties, which are fully correlated between cross-section measurements, are excluded.

		2–2.125	2.125–2.25	2.25–2.375	2.375–2.5	2.5–2.625	2.625–2.75	2.75–2.875	2.875–3	3–3.125	3.125–3.25	3.25–3.375	3.375–3.5	3.5–3.625	3.625–3.75	3.75–3.875	3.875–4	4–4.25	4.25–4.5	
η^μ	2–2.25	0.24	0.25	0.19	0.19	0.17	0.16	0.15	0.13	0.12	0.10	0.08	0.06	0.05	0.04	0.03	0.02	0.01	–	W^+
		0.22	0.23	0.17	0.17	0.16	0.15	0.13	0.12	0.11	0.09	0.07	0.05	0.04	0.04	0.03	0.02	0.01	–	W^-
	2.25–2.5	0.03	0.11	0.13	0.14	0.12	0.11	0.10	0.10	0.09	0.07	0.06	0.04	0.02	0.02	0.01	0.01	0.01	–	W^+
		0.03	0.10	0.12	0.13	0.11	0.10	0.10	0.09	0.08	0.07	0.06	0.04	0.02	0.02	0.01	0.01	0.00	–	W^-
	2.5–2.75	0.03	0.04	0.06	0.10	0.10	0.10	0.09	0.09	0.08	0.07	0.07	0.05	0.04	0.03	0.02	0.01	0.01	–	W^+
		0.03	0.03	0.06	0.10	0.09	0.09	0.08	0.08	0.08	0.07	0.06	0.05	0.04	0.02	0.02	0.01	0.01	–	W^-
	2.75–3	0.03	0.04	0.04	0.07	0.09	0.10	0.09	0.09	0.09	0.08	0.07	0.06	0.05	0.04	0.02	0.01	0.01	–	W^+
		0.02	0.03	0.03	0.05	0.07	0.07	0.07	0.07	0.06	0.06	0.04	0.04	0.04	0.03	0.01	0.01	0.01	–	W^-
	3–3.25	0.04	0.04	0.04	0.06	0.08	0.10	0.10	0.10	0.09	0.09	0.08	0.07	0.06	0.05	0.03	0.01	0.01	–	W^+
		0.03	0.04	0.03	0.05	0.06	0.08	0.08	0.08	0.08	0.07	0.07	0.06	0.05	0.04	0.02	0.01	0.01	–	W^-
	3.25–3.5	0.02	0.03	0.03	0.04	0.04	0.05	0.06	0.06	0.06	0.06	0.05	0.05	0.04	0.03	0.02	0.01	0.01	–	W^+
		0.02	0.02	0.02	0.03	0.03	0.04	0.05	0.05	0.05	0.04	0.04	0.03	0.03	0.02	0.02	0.01	0.00	–	W^-
	3.5–4	0.03	0.03	0.03	0.04	0.04	0.05	0.06	0.08	0.09	0.08	0.08	0.07	0.07	0.05	0.04	0.03	0.02	–	W^+
		0.03	0.03	0.03	0.04	0.04	0.05	0.06	0.08	0.09	0.09	0.08	0.07	0.06	0.05	0.04	0.03	0.02	–	W^-
	4–4.5	0.02	0.02	0.02	0.03	0.03	0.03	0.03	0.03	0.04	0.05	0.07	0.07	0.07	0.07	0.05	0.04	0.03	–	W^+
		0.02	0.02	0.02	0.03	0.03	0.03	0.03	0.03	0.04	0.05	0.07	0.07	0.06	0.07	0.04	0.03	0.03	–	W^-

Table 13. Correlation coefficients between differential cross-section measurements as a function of y_Z and W boson muon η. The LHC beam energy and luminosity uncertainties, which are fully correlated between cross-section measurements, are excluded.

References

[1] P.J. Rijken and W.L. van Neerven, *Order α_s^2 contributions to the Drell-Yan cross-section at fixed target energies*, *Phys. Rev.* **D 51** (1995) 44 [`hep-ph/9408366`] [ɪɴSPIRE].

[2] R. Hamberg, W.L. van Neerven and T. Matsuura, *A Complete calculation of the order α_s^2 correction to the Drell-Yan K factor*, *Nucl. Phys.* **B 359** (1991) 343 [*Erratum ibid.* **B 644** (2002) 403] [ɪɴSPIRE].

[3] W.L. van Neerven and E.B. Zijlstra, *The $O(\alpha_s^2)$ corrected Drell-Yan K factor in the DIS and MS scheme*, *Nucl. Phys.* **B 382** (1992) 11 [*Erratum ibid.* **B 680** (2004) 513] [ɪɴSPIRE].

[4] R.V. Harlander and W.B. Kilgore, *Next-to-next-to-leading order Higgs production at hadron colliders*, *Phys. Rev. Lett.* **88** (2002) 201801 [`hep-ph/0201206`] [ɪɴSPIRE].

[5] C. Anastasiou, L.J. Dixon, K. Melnikov and F. Petriello, *High precision QCD at hadron colliders: Electroweak gauge boson rapidity distributions at NNLO*, *Phys. Rev.* **D 69** (2004) 094008 [`hep-ph/0312266`] [ɪɴSPIRE].

[6] R.S. Thorne, A.D. Martin, W.J. Stirling and G. Watt, *Parton distributions and QCD at LHCb*, `arXiv:0808.1847`.

[7] LHCb collaboration, *Inclusive W and Z production in the forward region at $\sqrt{s} = 7$ TeV*, *JHEP* **06** (2012) 058 [`arXiv:1204.1620`] [ɪɴSPIRE].

[8] LHCb collaboration, *Measurement of the cross-section for $Z \to e^+e^-$ production in pp collisions at $\sqrt{s} = 7$ TeV*, *JHEP* **02** (2013) 106 [`arXiv:1212.4620`] [ɪɴSPIRE].

[9] LHCb collaboration, *A study of the Z production cross-section in pp collisions at $\sqrt{s} = 7$ TeV using tau final states*, *JHEP* **01** (2013) 111 [`arXiv:1210.6289`] [ɪɴSPIRE].

[10] LHCb collaboration, *Measurement of the forward W boson cross-section in pp collisions at $\sqrt{s} = 7$ TeV*, *JHEP* **12** (2014) 079 [`arXiv:1408.4354`] [ɪɴSPIRE].

[11] ATLAS collaboration, *Measurement of the inclusive $W^\pm$ and Z/γ^* cross sections in the e and μ decay channels in pp collisions at $\sqrt{s} = 7$ TeV with the ATLAS detector*, *Phys. Rev.* **D 85** (2012) 072004 [`arXiv:1109.5141`] [ɪɴSPIRE].

[12] CMS collaboration, *Measurement of the Inclusive W and Z Production Cross sections in pp Collisions at $\sqrt{s} = 7$ TeV*, *JHEP* **10** (2011) 132 [`arXiv:1107.4789`] [ɪɴSPIRE].

[13] A. Banfi, S. Redford, M. Vesterinen, P. Waller and T.R. Wyatt, *Optimisation of variables for studying dilepton transverse momentum distributions at hadron colliders*, *Eur. Phys. J.* **C 71** (2011) 1600 [`arXiv:1009.1580`] [ɪɴSPIRE].

[14] LHCb collaboration, *The LHCb Detector at the LHC*, 2008 *JINST* **3** S08005 [ɪɴSPIRE].

[15] LHCb collaboration, *LHCb Detector Performance*, *Int. J. Mod. Phys.* **A 30** (2015) 1530022 [`arXiv:1412.6352`] [ɪɴSPIRE].

[16] R. Aaij et al., *Performance of the LHCb Vertex Locator*, 2014 *JINST* **9** 09007 [`arXiv:1405.7808`] [ɪɴSPIRE].

[17] R. Arink et al., *Performance of the LHCb Outer Tracker*, 2014 *JINST* **9** P01002 [arXiv:1311.3893] [INSPIRE].

[18] M. Adinolfi et al., *Performance of the LHCb RICH detector at the LHC*, *Eur. Phys. J.* **C 73** (2013) 2431 [arXiv:1211.6759] [INSPIRE].

[19] A.A. Alves Jr. et al., *Performance of the LHCb muon system*, 2013 *JINST* **8** P02022 [arXiv:1211.1346] [INSPIRE].

[20] R. Aaij et al., *The LHCb Trigger and its Performance in 2011*, 2013 *JINST* **8** P04022 [arXiv:1211.3055] [INSPIRE].

[21] S. van der Meer, *Calibration of the effective beam height in the ISR*, ISR-PO/68-31 (1968).

[22] M. Ferro-Luzzi, *Proposal for an absolute luminosity determination in colliding beam experiments using vertex detection of beam-gas interactions*, *Nucl. Instrum. Meth.* **A 553** (2005) 388 [INSPIRE].

[23] LHCb collaboration, *Precision luminosity measurements at LHCb*, 2014 *JINST* **9** P12005 [arXiv:1410.0149] [INSPIRE].

[24] T. Sjöstrand, S. Mrenna and P.Z. Skands, *PYTHIA 6.4 Physics and Manual*, *JHEP* **05** (2006) 026 [hep-ph/0603175] [INSPIRE].

[25] T. Sjöstrand, S. Mrenna and P.Z. Skands, *A Brief Introduction to PYTHIA 8.1*, *Comput. Phys. Commun.* **178** (2008) 852 [arXiv:0710.3820] [INSPIRE].

[26] I. Belyaev et al., *Handling of the generation of primary events in Gauss, the LHCb simulation framework*, *IEEE Nucl. Sci. Symp. Conf. Rec.* (2010) 1155.

[27] P.M. Nadolsky et al., *Implications of CTEQ global analysis for collider observables*, *Phys. Rev.* **D 78** (2008) 013004 [arXiv:0802.0007] [INSPIRE].

[28] J. Pumplin, D.R. Stump, J. Huston, H.L. Lai, P.M. Nadolsky and W.K. Tung, *New generation of parton distributions with uncertainties from global QCD analysis*, *JHEP* **07** (2002) 012 [hep-ph/0201195] [INSPIRE].

[29] GEANT4 collaboration, S. Agostinelli et al., *GEANT4: A simulation toolkit*, *Nucl. Instrum. Meth.* **A 506** (2003) 250 [INSPIRE].

[30] Y. Li and F. Petriello, *Combining QCD and electroweak corrections to dilepton production in FEWZ*, *Phys. Rev.* **D 86** (2012) 094034 [arXiv:1208.5967] [INSPIRE].

[31] R. Gavin, Y. Li, F. Petriello and S. Quackenbush, *FEWZ 2.0: A code for hadronic Z production at next-to-next-to-leading order*, *Comput. Phys. Commun.* **182** (2011) 2388 [arXiv:1011.3540] [INSPIRE].

[32] S. Alekhin, J. Blümlein and S. Moch, *The ABM parton distributions tuned to LHC data*, *Phys. Rev.* **D 89** (2014) 054028 [arXiv:1310.3059] [INSPIRE].

[33] H.-L. Lai et al., *New parton distributions for collider physics*, *Phys. Rev.* **D 82** (2010) 074024 [arXiv:1007.2241] [INSPIRE].

[34] ZEUS, H1 collaborations, F.D. Aaron et al., *Combined Measurement and QCD Analysis of the Inclusive $e^{\pm}p$ Scattering Cross sections at HERA*, *JHEP* **01** (2010) 109 [arXiv:0911.0884] [INSPIRE].

[35] P. Jimenez-Delgado and E. Reya, *Dynamical NNLO parton distributions*, *Phys. Rev.* **D 79** (2009) 074023 [arXiv:0810.4274] [INSPIRE].

[36] A.D. Martin, W.J. Stirling, R.S. Thorne and G. Watt, *Parton distributions for the LHC*, *Eur. Phys. J.* **C 63** (2009) 189 [arXiv:0901.0002] [INSPIRE].

[37] NNPDF collaboration, R.D. Ball et al., *Parton distributions for the LHC Run II*, *JHEP* **04** (2015) 040 [arXiv:1410.8849] [INSPIRE].

[38] G.A. Ladinsky and C.P. Yuan, *The nonperturbative regime in QCD resummation for gauge boson production at hadron colliders*, *Phys. Rev.* **D 50** (1994) 4239 [hep-ph/9311341] [INSPIRE].

[39] C. Balázs and C.P. Yuan, *Soft gluon effects on lepton pairs at hadron colliders*, *Phys. Rev.* **D 56** (1997) 5558 [hep-ph/9704258] [INSPIRE].

[40] F. Landry, R. Brock, P.M. Nadolsky and C.P. Yuan, *Tevatron Run-1 Z boson data and Collins-Soper-Sterman resummation formalism*, *Phys. Rev.* **D 67** (2003) 073016 [hep-ph/0212159] [INSPIRE].

[41] P. Nason, *A new method for combining NLO QCD with shower Monte Carlo algorithms*, *JHEP* **11** (2004) 040 [hep-ph/0409146] [INSPIRE].

[42] G. Corcella et al., *HERWIG 6: An event generator for hadron emission reactions with interfering gluons (including supersymmetric processes)*, *JHEP* **01** (2001) 010 [hep-ph/0011363] [INSPIRE].

[43] G. Corcella et al., *HERWIG 6.5 release note*, hep-ph/0210213 [INSPIRE].

[44] S. Frixione and B.R. Webber, *Matching NLO QCD computations and parton shower simulations*, *JHEP* **06** (2002) 029 [hep-ph/0204244] [INSPIRE].

[45] S. Frixione, F. Stoeckli, P. Torrielli and B.R. Webber, *NLO QCD corrections in HERWIG++ with MC@NLO*, *JHEP* **01** (2011) 053 [arXiv:1010.0568] [INSPIRE].

[46] S. Joseph, S. Majhi, B.F.L. Ward and S.A. Yost, *HERWIRI1.0: MC Realization of IR-Improved DGLAP-CS Parton Showers*, *Phys. Lett.* **B 685** (2010) 283 [arXiv:0906.0788] [INSPIRE].

[47] S. Joseph, S. Majhi, B.F.L. Ward and S.A. Yost, *New Approach to Parton Shower MC's for Precision QCD Theory: HERWIRI 1.0(31)*, *Phys. Rev.* **D 81** (2010) 076008 [arXiv:1001.1434] [INSPIRE].

[48] S.K. Majhi, A. Mukhopadhyay, B.F.L. Ward and S.A. Yost, *Phenomenology of the Interplay between IR-Improved DGLAP-CS Theory and NLO ME Matched Parton Shower MC Precision*, *Phys. Lett.* **B 719** (2013) 367 [arXiv:1208.4750] [INSPIRE].

[49] B.F.L. Ward, *IR-Improved DGLAP Theory*, *Adv. High Energy Phys.* **2008** (2008) 682312.

[50] G. Altarelli and G. Parisi, *Asymptotic Freedom in Parton Language*, *Nucl. Phys.* **B 126** (1977) 298 [INSPIRE].

[51] Y.L. Dokshitzer, *Calculation of the Structure Functions for Deep Inelastic Scattering and e^+e^- Annihilation by Perturbation Theory in Quantum Chromodynamics.*, *Sov. Phys. JETP* **46** (1977) 641 [INSPIRE].

[52] L.N. Lipatov, *The parton model and perturbation theory*, *Sov. J. Nucl. Phys.* **20** (1975) 94 [*Yad. Fiz.* **20** (1974) 181] [INSPIRE].

[53] V.N. Gribov and L.N. Lipatov, *e^+e^- pair annihilation and deep inelastic e p scattering in perturbation theory*, *Sov. J. Nucl. Phys.* **15** (1972) 675 [INSPIRE].

[54] C.G. Callan Jr., *Broken scale invariance in scalar field theory*, *Phys. Rev.* **D 2** (1970) 1541 [INSPIRE].

[55] K. Symanzik, *Small distance behavior in field theory and power counting*, *Commun. Math. Phys.* **18** (1970) 227 [INSPIRE].

[56] K. Hamilton, P. Nason, E. Re and G. Zanderighi, *NNLOPS simulation of Higgs boson production*, *JHEP* **10** (2013) 222 [arXiv:1309.0017] [INSPIRE].

[57] ATLAS collaboration, *Measurement of the $Z \to \tau\tau$ Cross section with the ATLAS Detector*, *Phys. Rev.* **D 84** (2011) 112006 [arXiv:1108.2016] [INSPIRE].

[58] CMS collaboration, *Measurement of the Inclusive Z Cross section via Decays to Tau Pairs in pp Collisions at $\sqrt{s} = 7$ TeV*, *JHEP* **08** (2011) 117 [arXiv:1104.1617] [INSPIRE].

[59] ATLAS collaboration, *Measurement of the cross section for top-quark pair production in pp collisions at $\sqrt{s} = 7$ TeV with the ATLAS detector using final states with two high-p_T leptons*, *JHEP* **05** (2012) 059 [arXiv:1202.4892] [INSPIRE].

[60] CMS collaboration, *Measurement of the $t\bar{t}$ production cross section in the dilepton channel in pp collisions at $\sqrt{s} = 7$ TeV*, *JHEP* **11** (2012) 067 [arXiv:1208.2671] [INSPIRE].

[61] ATLAS collaboration, *Measurement of the WW cross section in $\sqrt{s} = 7$ TeV pp collisions with the ATLAS detector and limits on anomalous gauge couplings*, *Phys. Lett.* **B 712** (2012) 289 [arXiv:1203.6232] [INSPIRE].

[62] CMS collaboration, *Measurement of the W^+W^- Cross section in pp Collisions at $\sqrt{s} = 7$ TeV and Limits on Anomalous $WW\gamma$ and WWZ couplings*, *Eur. Phys. J.* **C 73** (2013) 2610 [arXiv:1306.1126] [INSPIRE].

[63] M. Bahr et al., *HERWIG++ Physics and Manual*, *Eur. Phys. J.* **C 58** (2008) 639 [arXiv:0803.0883] [INSPIRE].

[64] T. Adye, *Unfolding algorithms and tests using RooUnfold*, in proceedings of *The PHYSTAT 2011 workshop on statistical issues related to discovery claims in search experiments and unfolding*, H.B. Prosper and L. Lyons eds., CERN, Geneva, Switzerland, January 2011, arXiv:1105.1160 [INSPIRE].

[65] G. D'Agostini, *A multidimensional unfolding method based on Bayes' theorem*, *Nucl. Instrum. Meth.* **A 362** (1995) 487 [INSPIRE].

[66] A. Hocker and V. Kartvelishvili, *SVD approach to data unfolding*, *Nucl. Instrum. Meth.* **A 372** (1996) 469 [hep-ph/9509307] [INSPIRE].

[67] G. Cowan, *Statistical data analysis*, Oxford University Press, (1998).

[68] S. Frixione, P. Nason and C. Oleari, *Matching NLO QCD computations with Parton Shower simulations: the POWHEG method*, *JHEP* **11** (2007) 070 [arXiv:0709.2092] [INSPIRE].

[69] S. Alioli, P. Nason, C. Oleari and E. Re, *A general framework for implementing NLO calculations in shower Monte Carlo programs: the POWHEG BOX*, *JHEP* **06** (2010) 043 [arXiv:1002.2581] [INSPIRE].

[70] J. Wenninger, *Energy calibration of the LHC beams at 4 TeV*, Tech. Rep. CERN-ATS-2013-040, CERN, (2013).

[71] S. Catani, L. Cieri, G. Ferrera, D. de Florian and M. Grazzini, *Vector boson production at hadron colliders: a fully exclusive QCD calculation at NNLO*, *Phys. Rev. Lett.* **103** (2009) 082001 [arXiv:0903.2120] [INSPIRE].

The LHCb collaboration

R. Aaij[38], B. Adeva[37], M. Adinolfi[46], A. Affolder[52], Z. Ajaltouni[5], S. Akar[6], J. Albrecht[9],
F. Alessio[38], M. Alexander[51], S. Ali[41], G. Alkhazov[30], P. Alvarez Cartelle[53], A.A. Alves Jr[57],
S. Amato[2], S. Amerio[22], Y. Amhis[7], L. An[3], L. Anderlini[17,g], J. Anderson[40], M. Andreotti[16,f],
J.E. Andrews[58], R.B. Appleby[54], O. Aquines Gutierrez[10], F. Archilli[38], P. d'Argent[11],
A. Artamonov[35], M. Artuso[59], E. Aslanides[6], G. Auriemma[25,n], M. Baalouch[5], S. Bachmann[11],
J.J. Back[48], A. Badalov[36], C. Baesso[60], W. Baldini[16,38], R.J. Barlow[54], C. Barschel[38], S. Barsuk[7],
W. Barter[38], V. Batozskaya[28], V. Battista[39], A. Bay[39], L. Beaucourt[4], J. Beddow[51],
F. Bedeschi[23], I. Bediaga[1], L.J. Bel[41], I. Belyaev[31], E. Ben-Haim[8], G. Bencivenni[18], S. Benson[38],
J. Benton[46], A. Berezhnoy[32], R. Bernet[40], A. Bertolin[22], M.-O. Bettler[38], M. van Beuzekom[41],
A. Bien[11], S. Bifani[45], T. Bird[54], A. Birnkraut[9], A. Bizzeti[17,i], T. Blake[48], F. Blanc[39], J. Blouw[10],
S. Blusk[59], V. Bocci[25], A. Bondar[34], N. Bondar[30,38], W. Bonivento[15], S. Borghi[54], A. Borgia[59],
M. Borsato[7], T.J.V. Bowcock[52], E. Bowen[40], C. Bozzi[16], D. Brett[54], M. Britsch[10], T. Britton[59],
J. Brodzicka[54], N.H. Brook[46], A. Bursche[40], J. Buytaert[38], S. Cadeddu[15], R. Calabrese[16,f],
M. Calvi[20,k], M. Calvo Gomez[36,p], P. Campana[18], D. Campora Perez[38], L. Capriotti[54],
A. Carbone[14,d], G. Carboni[24,l], R. Cardinale[19,j], A. Cardini[15], P. Carniti[20], L. Carson[50],
K. Carvalho Akiba[2,38], R. Casanova Mohr[36], G. Casse[52], L. Cassina[20,k], L. Castillo Garcia[38],
M. Cattaneo[38], Ch. Cauet[9], G. Cavallero[19], R. Cenci[23,t], M. Charles[8], Ph. Charpentier[38],
M. Chefdeville[4], S. Chen[54], S.-F. Cheung[55], N. Chiapolini[40], M. Chrzaszcz[40,26], X. Cid Vidal[38],
G. Ciezarek[41], P.E.L. Clarke[50], M. Clemencic[38], H.V. Cliff[47], J. Closier[38], V. Coco[38], J. Cogan[6],
E. Cogneras[5], V. Cogoni[15,e], L. Cojocariu[29], G. Collazuol[22], P. Collins[38], A. Comerma-Montells[11],
A. Contu[15,38], A. Cook[46], M. Coombes[46], S. Coquereau[8], G. Corti[38], M. Corvo[16,f], I. Counts[56],
B. Couturier[38], G.A. Cowan[50], D.C. Craik[48], A. Crocombe[48], M. Cruz Torres[60], S. Cunliffe[53],
R. Currie[53], C. D'Ambrosio[38], J. Dalseno[46], P.N.Y. David[41], A. Davis[57], K. De Bruyn[41],
S. De Capua[54], M. De Cian[11], J.M. De Miranda[1], L. De Paula[2], W. De Silva[57], P. De Simone[18],
C.-T. Dean[51], D. Decamp[4], M. Deckenhoff[9], L. Del Buono[8], N. Déléage[4], D. Derkach[55],
O. Deschamps[5], F. Dettori[38], B. Dey[40], A. Di Canto[38], F. Di Ruscio[24], H. Dijkstra[38],
S. Donleavy[52], F. Dordei[11], M. Dorigo[39], A. Dosil Suárez[37], D. Dossett[48], A. Dovbnya[43],
K. Dreimanis[52], G. Dujany[54], F. Dupertuis[39], P. Durante[38], R. Dzhelyadin[35], A. Dziurda[26],
A. Dzyuba[30], S. Easo[49,38], U. Egede[53], V. Egorychev[31], S. Eidelman[34], S. Eisenhardt[50],
U. Eitschberger[9], R. Ekelhof[9], L. Eklund[51], I. El Rifai[5], Ch. Elsasser[40], S. Ely[59], S. Esen[11],
H.M. Evans[47], T. Evans[55], A. Falabella[14], C. Färber[11], C. Farinelli[41], N. Farley[45], S. Farry[52],
R. Fay[52], D. Ferguson[50], V. Fernandez Albor[37], F. Ferrari[14], F. Ferreira Rodrigues[1],
M. Ferro-Luzzi[38], S. Filippov[33], M. Fiore[16,38,f], M. Fiorini[16,f], M. Firlej[27], C. Fitzpatrick[39],
T. Fiutowski[27], P. Fol[53], M. Fontana[10], F. Fontanelli[19,j], R. Forty[38], O. Francisco[2], M. Frank[38],
C. Frei[38], M. Frosini[17], J. Fu[21,38], E. Furfaro[24,l], A. Gallas Torreira[37], D. Galli[14,d],
S. Gallorini[22,38], S. Gambetta[19,j], M. Gandelman[2], P. Gandini[59], Y. Gao[3], J. García Pardiñas[37],
J. Garofoli[59], J. Garra Tico[47], L. Garrido[36], D. Gascon[36], C. Gaspar[38], U. Gastaldi[16], R. Gauld[55],
L. Gavardi[9], G. Gazzoni[5], A. Geraci[21,v], D. Gerick[11], E. Gersabeck[11], M. Gersabeck[54],
T. Gershon[48], Ph. Ghez[4], A. Gianelle[22], S. Gianì[39], V. Gibson[47], L. Giubega[29], V.V. Gligorov[38],
C. Göbel[60], D. Golubkov[31], A. Golutvin[53,31,38], A. Gomes[1,a], C. Gotti[20,k],
M. Grabalosa Gándara[5], R. Graciani Diaz[36], L.A. Granado Cardoso[38], E. Graugés[36],
E. Graverini[40], G. Graziani[17], A. Grecu[29], E. Greening[55], S. Gregson[47], P. Griffith[45], L. Grillo[11],
O. Grünberg[63], B. Gui[59], E. Gushchin[33], Yu. Guz[35,38], T. Gys[38], C. Hadjivasiliou[59], G. Haefeli[39],
C. Haen[38], S.C. Haines[47], S. Hall[53], B. Hamilton[58], T. Hampson[46], X. Han[11],
S. Hansmann-Menzemer[11], N. Harnew[55], S.T. Harnew[46], J. Harrison[54], J. He[38], T. Head[39],
V. Heijne[41], K. Hennessy[52], P. Henrard[5], L. Henry[8], J.A. Hernando Morata[37],

E. van Herwijnen[38], M. Heß[63], A. Hicheur[2], D. Hill[55], M. Hoballah[5], C. Hombach[54],
W. Hulsbergen[41], T. Humair[53], N. Hussain[55], D. Hutchcroft[52], D. Hynds[51], M. Idzik[27], P. Ilten[56],
R. Jacobsson[38], A. Jaeger[11], J. Jalocha[55], E. Jans[41], A. Jawahery[58], F. Jing[3], M. John[55],
D. Johnson[38], C.R. Jones[47], C. Joram[38], B. Jost[38], N. Jurik[59], S. Kandybei[43], W. Kanso[6],
M. Karacson[38], T.M. Karbach[38,†], S. Karodia[51], M. Kelsey[59], I.R. Kenyon[45], M. Kenzie[38],
T. Ketel[42], B. Khanji[20,38,k], C. Khurewathanakul[39], S. Klaver[54], K. Klimaszewski[28],
O. Kochebina[7], M. Kolpin[11], I. Komarov[39], R.F. Koopman[42], P. Koppenburg[41,38], M. Korolev[32],
L. Kravchuk[33], K. Kreplin[11], M. Kreps[48], G. Krocker[11], P. Krokovny[34], F. Kruse[9],
W. Kucewicz[26,o], M. Kucharczyk[26], V. Kudryavtsev[34], K. Kurek[28], T. Kvaratskheliya[31],
V.N. La Thi[39], D. Lacarrere[38], G. Lafferty[54], A. Lai[15], D. Lambert[50], R.W. Lambert[42],
G. Lanfranchi[18], C. Langenbruch[48], B. Langhans[38], T. Latham[48], C. Lazzeroni[45], R. Le Gac[6],
J. van Leerdam[41], J.-P. Lees[4], R. Lefèvre[5], A. Leflat[32], J. Lefrançois[7], O. Leroy[6], T. Lesiak[26],
B. Leverington[11], Y. Li[7], T. Likhomanenko[64], M. Liles[52], R. Lindner[38], C. Linn[38], F. Lionetto[40],
B. Liu[15], S. Lohn[38], I. Longstaff[51], J.H. Lopes[2], P. Lowdon[40], D. Lucchesi[22,r], H. Luo[50],
A. Lupato[22], E. Luppi[16,f], O. Lupton[55], F. Machefert[7], I.V. Machikhiliyan[31], F. Maciuc[29],
O. Maev[30], S. Malde[55], A. Malinin[64], G. Manca[15,e], G. Mancinelli[6], P. Manning[59], A. Mapelli[38],
J. Maratas[5], J.F. Marchand[4], U. Marconi[14], C. Marin Benito[36], P. Marino[23,38,t], R. Märki[39],
J. Marks[11], G. Martellotti[25], M. Martinelli[39], D. Martinez Santos[42], F. Martinez Vidal[66],
D. Martins Tostes[2], A. Massafferri[1], R. Matev[38], Z. Mathe[38], C. Matteuzzi[20], A. Mauri[40],
B. Maurin[39], A. Mazurov[45], M. McCann[53], J. McCarthy[45], A. McNab[54], R. McNulty[12],
B. McSkelly[52], B. Meadows[57], F. Meier[9], M. Meissner[11], M. Merk[41], D.A. Milanes[62],
M.-N. Minard[4], D.S. Mitzel[11], J. Molina Rodriguez[60], S. Monteil[5], M. Morandin[22], P. Morawski[27],
A. Mordà[6], M.J. Morello[23,t], J. Moron[27], A.B. Morris[50], R. Mountain[59], F. Muheim[50], J. Müller[9],
K. Müller[40], V. Müller[9], M. Mussini[14], B. Muster[39], P. Naik[46], T. Nakada[39], R. Nandakumar[49],
I. Nasteva[2], M. Needham[50], N. Neri[21], S. Neubert[11], N. Neufeld[38], M. Neuner[11], A.D. Nguyen[39],
T.D. Nguyen[39], C. Nguyen-Mau[39,q], V. Niess[5], R. Niet[9], N. Nikitin[32], T. Nikodem[11],
A. Novoselov[35], D.P. O'Hanlon[48], A. Oblakowska-Mucha[27], V. Obraztsov[35], S. Ogilvy[51],
O. Okhrimenko[44], R. Oldeman[15,e], C.J.G. Onderwater[67], B. Osorio Rodrigues[1],
J.M. Otalora Goicochea[2], A. Otto[38], P. Owen[53], A. Oyanguren[66], A. Palano[13,c], F. Palombo[21,u],
M. Palutan[18], J. Panman[38], A. Papanestis[49], M. Pappagallo[51], L.L. Pappalardo[16,f], C. Parkes[54],
G. Passaleva[17], G.D. Patel[52], M. Patel[53], C. Patrignani[19,j], A. Pearce[54,49], A. Pellegrino[41],
G. Penso[25,m], M. Pepe Altarelli[38], S. Perazzini[14,d], P. Perret[5], L. Pescatore[45], K. Petridis[46],
A. Petrolini[19,j], M. Petruzzo[21], E. Picatoste Olloqui[36], B. Pietrzyk[4], T. Pilař[48], D. Pinci[25],
A. Pistone[19], S. Playfer[50], M. Plo Casasus[37], T. Poikela[38], F. Polci[8], A. Poluektov[48,34],
I. Polyakov[31], E. Polycarpo[2], A. Popov[35], D. Popov[10], B. Popovici[29], C. Potterat[2], E. Price[46],
J.D. Price[52], J. Prisciandaro[39], A. Pritchard[52], C. Prouve[46], V. Pugatch[44], A. Puig Navarro[39],
G. Punzi[23,s], W. Qian[4], R. Quagliani[7,46], B. Rachwal[26], J.H. Rademacker[46],
B. Rakotomiaramanana[39], M. Rama[23], M.S. Rangel[2], I. Raniuk[43], N. Rauschmayr[38], G. Raven[42],
F. Redi[53], S. Reichert[54], M.M. Reid[48], A.C. dos Reis[1], S. Ricciardi[49], S. Richards[46], M. Rihl[38],
K. Rinnert[52], V. Rives Molina[36], P. Robbe[7,38], A.B. Rodrigues[1], E. Rodrigues[54],
P. Rodriguez Perez[54], S. Roiser[38], V. Romanovsky[35], A. Romero Vidal[37], M. Rotondo[22],
J. Rouvinet[39], T. Ruf[38], H. Ruiz[36], P. Ruiz Valls[66], J.J. Saborido Silva[37], N. Sagidova[30], P. Sail[51],
B. Saitta[15,e], V. Salustino Guimaraes[2], C. Sanchez Mayordomo[66], B. Sanmartin Sedes[37],
R. Santacesaria[25], C. Santamarina Rios[37], E. Santovetti[24,l], A. Sarti[18,m], C. Satriano[25,n],
A. Satta[24], D.M. Saunders[46], D. Savrina[31,32], M. Schiller[38], H. Schindler[38], M. Schlupp[9],
M. Schmelling[10], T. Schmelzer[9], B. Schmidt[38], O. Schneider[39], A. Schopper[38], M.-H. Schune[7],
R. Schwemmer[38], B. Sciascia[18], A. Sciubba[25,m], A. Semennikov[31], I. Sepp[53], N. Serra[40],
J. Serrano[6], L. Sestini[22], P. Seyfert[11], M. Shapkin[35], I. Shapoval[16,43,f], Y. Shcheglov[30],

T. Shears[52], L. Shekhtman[34], V. Shevchenko[64], A. Shires[9], R. Silva Coutinho[48], G. Simi[22],
M. Sirendi[47], N. Skidmore[46], I. Skillicorn[51], T. Skwarnicki[59], E. Smith[55,49], E. Smith[53],
J. Smith[47], M. Smith[54], H. Snoek[41], M.D. Sokoloff[57,38], F.J.P. Soler[51], F. Soomro[39], D. Souza[46],
B. Souza De Paula[2], B. Spaan[9], P. Spradlin[51], S. Sridharan[38], F. Stagni[38], M. Stahl[11], S. Stahl[38],
O. Steinkamp[40], O. Stenyakin[35], F. Sterpka[59], S. Stevenson[55], S. Stoica[29], S. Stone[59],
B. Storaci[40], S. Stracka[23,t], M. Straticiuc[29], U. Straumann[40], R. Stroili[22], L. Sun[57], W. Sutcliffe[53],
K. Swientek[27], S. Swientek[9], V. Syropoulos[42], M. Szczekowski[28], P. Szczypka[39,38], T. Szumlak[27],
S. T'Jampens[4], T. Tekampe[9], M. Teklishyn[7], G. Tellarini[16,f], F. Teubert[38], C. Thomas[55],
E. Thomas[38], J. van Tilburg[41], V. Tisserand[4], M. Tobin[39], J. Todd[57], S. Tolk[42],
L. Tomassetti[16,f], D. Tonelli[38], S. Topp-Joergensen[55], N. Torr[55], E. Tournefier[4], S. Tourneur[39],
K. Trabelsi[39], M.T. Tran[39], M. Tresch[40], A. Trisovic[38], A. Tsaregorodtsev[6], P. Tsopelas[41],
N. Tuning[41,38], M. Ubeda Garcia[38], A. Ukleja[28], A. Ustyuzhanin[65,64], U. Uwer[11], C. Vacca[15,e],
V. Vagnoni[14], G. Valenti[14], A. Vallier[7], R. Vazquez Gomez[18], P. Vazquez Regueiro[37],
C. Vázquez Sierra[37], S. Vecchi[16], J.J. Velthuis[46], M. Veltri[17,h], G. Veneziano[39], M. Vesterinen[11],
B. Viaud[7], D. Vieira[2], M. Vieites Diaz[37], X. Vilasis-Cardona[36,p], A. Vollhardt[40], D. Volyanskyy[10],
D. Voong[46], A. Vorobyev[30], V. Vorobyev[34], C. Voß[63], J.A. de Vries[41], R. Waldi[63], C. Wallace[48],
R. Wallace[12], J. Walsh[23], S. Wandernoth[11], J. Wang[59], D.R. Ward[47], N.K. Watson[45],
D. Websdale[53], A. Weiden[40], M. Whitehead[48], D. Wiedner[11], G. Wilkinson[55,38], M. Wilkinson[59],
M. Williams[38], M.P. Williams[45], M. Williams[56], F.F. Wilson[49], J. Wimberley[58], J. Wishahi[9],
W. Wislicki[28], M. Witek[26], G. Wormser[7], S.A. Wotton[47], S. Wright[47], K. Wyllie[38], Y. Xie[61],
Z. Xu[39], Z. Yang[3], X. Yuan[34], O. Yushchenko[35], M. Zangoli[14], M. Zavertyaev[10,b], L. Zhang[3],
Y. Zhang[3], A. Zhelezov[11], A. Zhokhov[31], L. Zhong[3]

1   Centro Brasileiro de Pesquisas Físicas (CBPF), Rio de Janeiro, Brazil
2   Universidade Federal do Rio de Janeiro (UFRJ), Rio de Janeiro, Brazil
3   Center for High Energy Physics, Tsinghua University, Beijing, China
4   LAPP, Université Savoie Mont-Blanc, CNRS/IN2P3, Annecy-Le-Vieux, France
5   Clermont Université, Université Blaise Pascal, CNRS/IN2P3, LPC, Clermont-Ferrand, France
6   CPPM, Aix-Marseille Université, CNRS/IN2P3, Marseille, France
7   LAL, Université Paris-Sud, CNRS/IN2P3, Orsay, France
8   LPNHE, Université Pierre et Marie Curie, Université Paris Diderot, CNRS/IN2P3, Paris, France
9   Fakultät Physik, Technische Universität Dortmund, Dortmund, Germany
10 Max-Planck-Institut für Kernphysik (MPIK), Heidelberg, Germany
11 Physikalisches Institut, Ruprecht-Karls-Universität Heidelberg, Heidelberg, Germany
12 School of Physics, University College Dublin, Dublin, Ireland
13 Sezione INFN di Bari, Bari, Italy
14 Sezione INFN di Bologna, Bologna, Italy
15 Sezione INFN di Cagliari, Cagliari, Italy
16 Sezione INFN di Ferrara, Ferrara, Italy
17 Sezione INFN di Firenze, Firenze, Italy
18 Laboratori Nazionali dell'INFN di Frascati, Frascati, Italy
19 Sezione INFN di Genova, Genova, Italy
20 Sezione INFN di Milano Bicocca, Milano, Italy
21 Sezione INFN di Milano, Milano, Italy
22 Sezione INFN di Padova, Padova, Italy
23 Sezione INFN di Pisa, Pisa, Italy
24 Sezione INFN di Roma Tor Vergata, Roma, Italy
25 Sezione INFN di Roma La Sapienza, Roma, Italy
26 Henryk Niewodniczanski Institute of Nuclear Physics Polish Academy of Sciences, Kraków, Poland
27 AGH - University of Science and Technology, Faculty of Physics and Applied Computer Science,
    Kraków, Poland

[28] National Center for Nuclear Research (NCBJ), Warsaw, Poland

[29] Horia Hulubei National Institute of Physics and Nuclear Engineering, Bucharest-Magurele, Romania

[30] Petersburg Nuclear Physics Institute (PNPI), Gatchina, Russia

[31] Institute of Theoretical and Experimental Physics (ITEP), Moscow, Russia

[32] Institute of Nuclear Physics, Moscow State University (SINP MSU), Moscow, Russia

[33] Institute for Nuclear Research of the Russian Academy of Sciences (INR RAN), Moscow, Russia

[34] Budker Institute of Nuclear Physics (SB RAS) and Novosibirsk State University, Novosibirsk, Russia

[35] Institute for High Energy Physics (IHEP), Protvino, Russia

[36] Universitat de Barcelona, Barcelona, Spain

[37] Universidad de Santiago de Compostela, Santiago de Compostela, Spain

[38] European Organization for Nuclear Research (CERN), Geneva, Switzerland

[39] Ecole Polytechnique Fédérale de Lausanne (EPFL), Lausanne, Switzerland

[40] Physik-Institut, Universität Zürich, Zürich, Switzerland

[41] Nikhef National Institute for Subatomic Physics, Amsterdam, The Netherlands

[42] Nikhef National Institute for Subatomic Physics and VU University Amsterdam, Amsterdam, The Netherlands

[43] NSC Kharkiv Institute of Physics and Technology (NSC KIPT), Kharkiv, Ukraine

[44] Institute for Nuclear Research of the National Academy of Sciences (KINR), Kyiv, Ukraine

[45] University of Birmingham, Birmingham, United Kingdom

[46] H.H. Wills Physics Laboratory, University of Bristol, Bristol, United Kingdom

[47] Cavendish Laboratory, University of Cambridge, Cambridge, United Kingdom

[48] Department of Physics, University of Warwick, Coventry, United Kingdom

[49] STFC Rutherford Appleton Laboratory, Didcot, United Kingdom

[50] School of Physics and Astronomy, University of Edinburgh, Edinburgh, United Kingdom

[51] School of Physics and Astronomy, University of Glasgow, Glasgow, United Kingdom

[52] Oliver Lodge Laboratory, University of Liverpool, Liverpool, United Kingdom

[53] Imperial College London, London, United Kingdom

[54] School of Physics and Astronomy, University of Manchester, Manchester, United Kingdom

[55] Department of Physics, University of Oxford, Oxford, United Kingdom

[56] Massachusetts Institute of Technology, Cambridge, MA, United States

[57] University of Cincinnati, Cincinnati, OH, United States

[58] University of Maryland, College Park, MD, United States

[59] Syracuse University, Syracuse, NY, United States

[60] Pontifícia Universidade Católica do Rio de Janeiro (PUC-Rio), Rio de Janeiro, Brazil, associated to [2]

[61] Institute of Particle Physics, Central China Normal University, Wuhan, Hubei, China, associated to [3]

[62] Departamento de Fisica, Universidad Nacional de Colombia, Bogota, Colombia, associated to [8]

[63] Institut für Physik, Universität Rostock, Rostock, Germany, associated to [11]

[64] National Research Centre Kurchatov Institute, Moscow, Russia, associated to [31]

[65] Yandex School of Data Analysis, Moscow, Russia, associated to [31]

[66] Instituto de Fisica Corpuscular (IFIC), Universitat de Valencia-CSIC, Valencia, Spain, associated to [36]

[67] Van Swinderen Institute, University of Groningen, Groningen, The Netherlands, associated to [41]

[a] Universidade Federal do Triângulo Mineiro (UFTM), Uberaba-MG, Brazil

[b] P.N. Lebedev Physical Institute, Russian Academy of Science (LPI RAS), Moscow, Russia

[c] Università di Bari, Bari, Italy

[d] Università di Bologna, Bologna, Italy

[e] Università di Cagliari, Cagliari, Italy

[f] Università di Ferrara, Ferrara, Italy

^{g} Università di Firenze, Firenze, Italy

^{h} Università di Urbino, Urbino, Italy

^{i} Università di Modena e Reggio Emilia, Modena, Italy

^{j} Università di Genova, Genova, Italy

^{k} Università di Milano Bicocca, Milano, Italy

^{l} Università di Roma Tor Vergata, Roma, Italy

^{m} Università di Roma La Sapienza, Roma, Italy

^{n} Università della Basilicata, Potenza, Italy

^{o} AGH - University of Science and Technology, Faculty of Computer Science,
Electronics and Telecommunications, Kraków, Poland

^{p} LIFAELS, La Salle, Universitat Ramon Llull, Barcelona, Spain

^{q} Hanoi University of Science, Hanoi, Viet Nam

^{r} Università di Padova, Padova, Italy

^{s} Università di Pisa, Pisa, Italy

^{t} Scuola Normale Superiore, Pisa, Italy

^{u} Università degli Studi di Milano, Milano, Italy

^{v} Politecnico di Milano, Milano, Italy

† Deceased